DANMARKS OG GRØNLANDS GEOLOGISKE UNDERSØGELSE RAPPORT 2009/77

PROMICE 2007 - 2008

Status Report for the first two years of the Programme for Monitoring of the Greenland Ice Sheet

Andreas P. Ahlstrøm, Dirk van As, Michele Citterio, Signe Bech Andersen, Faezeh Maghami Nick, Peter Gravesen, Karen Edelvang, Robert S. Fausto, Steen Savstrup Kristensen, Erik Lintz Christensen, John P. Merryman Boncori, Jørgen Dall, Rene Forsberg, Lars Stenseng, Susanne Hanson & Dorthe Petersen

GEOLOGICAL SURVEY OF DENMARK AND GREENLAND
MINISTRY OF CLIMATE AND ENERGY

GEUS

PROMICE 2007 - 2008

Status Report for the first two years of the Programme for Monitoring of the Greenland Ice Sheet

Andreas P. Ahlstrøm[1], Dirk van As[1], Michele Citterio[1],
Signe Bech Andersen[1], Faezeh Maghami Nick[1],
Peter Gravesen[1], Karen Edelvang[1], Robert S. Fausto[1],
Steen Savstrup Kristensen[2], Erik Lintz Christensen[2],
John P. Merryman Boncori[2], Jørgen Dall[2],
Rene Forsberg[2], Lars Stenseng[2],
Susanne Hanson[2] & Dorthe Petersen[3]

[1] De Nationale Geologiske Undersøgelser for Danmark og Grønland (GEUS)
[2] DTU-Space
[3] ASIAQ

GEOLOGICAL SURVEY OF DENMARK AND GREENLAND
MINISTRY OF CLIMATE AND ENERGY

GEUS

Contents

Introduction

This report documents the progress of the Programme for Monitoring of the Greenland Ice Sheet (PROMICE) in 2007-2008.

The Programme is funded by the Ministry of Climate and Energy through the Danish Cooperation for Environment in the Arctic (DANCEA) administered by the Danish Energy Agency (Energistyrelsen). The grant refers to J.nr. MST 112-001336 (journal number of the Danish Environmental Agency) and is administered by Morten Skovgård Olsen at the Danish Energy Agency.

The report broadly follows the original project description, although it is not specifically divided in separate years. For a few activities, descriptions of work spreading into 2009 (that is after the period 2007-2008 that this report officially reports) have been included to obtain a meaningful chapter.

Purchase and calibration of instruments

One of the first tasks in PROMICE was to ensure the establishing of a network of automatic stations, measuring weather and ice-sheet surface mass-balance. The glaciology group at GEUS already had a long experience in building and maintaining such stations, but the whole production line and maintenance plan was revised to facilitate the larger scale of the new monitoring programme. At GEUS, a technician was allocated a full-time position to form the backbone of this part of PROMICE. Thus we now have a flowing work plan for purchase of parts and instruments, modification of instruments, assembly of stations, testing of modified instruments, programming of data loggers, testing of complete stations set-ups and finally shipment to relevant ports or airports in Greenland. An updated list of suppliers complete with personal contacts is part of the common project space. A previously developed MS Access database (GlacioBase) has been used to keep track of all instruments and meta-data, but will be ported to our new central PROMICE database by the end of 2009.

Each sensor on the PROMICE stations either outputs useable physical quantities, or is provided with calibration coefficients by the manufacturer. The only sensor we determine an extra set of calibration coefficients for before placing it in the field, is for the pressure transducer assembly. This is because we use the transducer in different conditions than it was designed for (i.e. in an anti-freeze mixture in a hose drilled into ice, as opposed to in water) and because there are reports of pressure transducer output experiencing a substantial drift. Table 1 shows that before installation on the ice the GEUS and manufacturer calibration coefficients are virtually identical, with differences less than 1.5%.

Serial number pressure transducer	Location	Antifreeze %	Density for antifreeze mixture (kg/m3)	GEUS coefficient (m/mV)	Manufacturer coefficient (m/mV)	Difference (%)
591	KPC_U	100	1145	1.06274	1.07579	-1.2
595	KAN_L	100	1145	1.11717	1.11821	-0.1
5112	KPC_L	100	1145	1.10137	1.10071	0.1
5113	QAS_U	100	1145	1.09706	1.08446	1.2
5114	SCO_L	100	1145	1.10256	1.11019	-0.7
5116	QAS_L	50	1092	1.16261	1.14652	1.4
5135	UPE_U	50	1092	1.15811	1.15662	0.1
5137	UPE_L	50	1092	1.16939	1.16428	0.4
5138	MIT	50	1092	1.10826	1.10396	0.4

Table 1. *Calibration coefficients for the pressure transducers.*

Recalibration is performed upon return. Sensors that have been damaged in the field or are suspected to give unreliable results are shipped back to the manufacturer for repair and recalibration. The remainder of the sensors will be recalibrated by GEUS personnel. Whereas the air pressure, humidity, ablation / surface height, tilt, and orientation can be checked and/or recalibrated at GEUS, the radiation, wind, and temperature sensors require placement outdoors to capture the atmosphere’s variability. We are developing a set-up at a test site of the Danish Meteorological Institute, at which we can install multiple identical sensors simultaneously to compare readings. Wind speed sensors (which will have the bearings in the propeller shaft replaced at GEUS) and temperature sensors will be compared to the high-quality DMI data and either considered functional or send to the manufacturer. The radiation sensors will also undergo intercomparison with DMI data, with the goal to produce new calibration coefficients. If the automatic measurement frequency of the test set-up is high enough (for instance measuring every five minutes), one week of testing will suffice.

Table 2 gives an overview of the sensors, with the intended frequency of recalibration. The recalibration frequency is strongly dependent on the frequency of the station visits. If a station cannot be visited due to financial, logistical, or other reasons in the year that one or more sensors need recalibration, the recalibration will be delayed until the next visit.

Measured parameter	Sensor	Calibration frequency	Place of calibration	Method
radiation	Kipp & Zonen CNR1	every 2 years	Denmark, outdoors	determining new coefficients
Wind	Young	every 2 years	Denmark, outdoors	check of accuracy
temperature	Rotronic MP100H	every 3 years	Denmark, outdoors	check of accuracy
humidity	Rotronic HygroClip	every year	GEUS	digital recalibration
Ablation	Ørum & Jensen NT1400	when melted out (>2 years)	GEUS	determining new coefficients
surface height	Campbell SR50	every 3 years	GEUS	check of accuracy
ice temperature	home-made	when melted out (>1 year)	GEUS	check of accuracy
tilt	HL-Planar NS25/E2	every 3 years	GEUS	determining new coefficients
orientation	in development	every 3 years	GEUS	check of accuracy
air pressure	Campbell CS100	every 3 years	GEUS	check of accuracy

Table 2. *Calibration plan for the sensors mounted on the stations.*

Assembling and testing automatic weather stations

After the equipment needed to build a weather station has arrived, we start the construction process. First step is to produce a set of steel wiring for the aluminum tripod. The tripod with all components (wires, shackles, kee clamps, wire tightener, etc.) is then constructed in the GEUS courtyard for testing purposes.

Figure 1. *Wiring of instruments, power and data transmission in the GEUS Glaciology Workshop.*

The sensors, battery enclosure, solar panel, Iridium antenna, and logger enclosure are wired up in the technician's office (see Figure 1). It takes a few days to wire up all equipment for one AWS. Most time-consuming to construct is the logger enclosure (see Figure 2). Also a considerable amount of time needs to be spent on the Rotronics assembly, which holds the temperature and relative humidity sensors, the thermistor string, and the pressure transducer assembly. The thermistor string is equipment that needs to be made to our exact specifications and up to this moment cannot be ordered from elsewhere. The thermistor string is thus custom-built from raw materials at GEUS. For the details of its construction, see Table 3. The construction of the pressure transducer assembly involves inserting the pressure transducer and wire in the hose, sealing it at the bottom with a weight, attaching a T-piece at the top end, connecting a plug and overflow bladder, and filling the system with an antifreeze mixture. Hereafter, the pressure transducer output is calibrated as mentioned in the previous section.

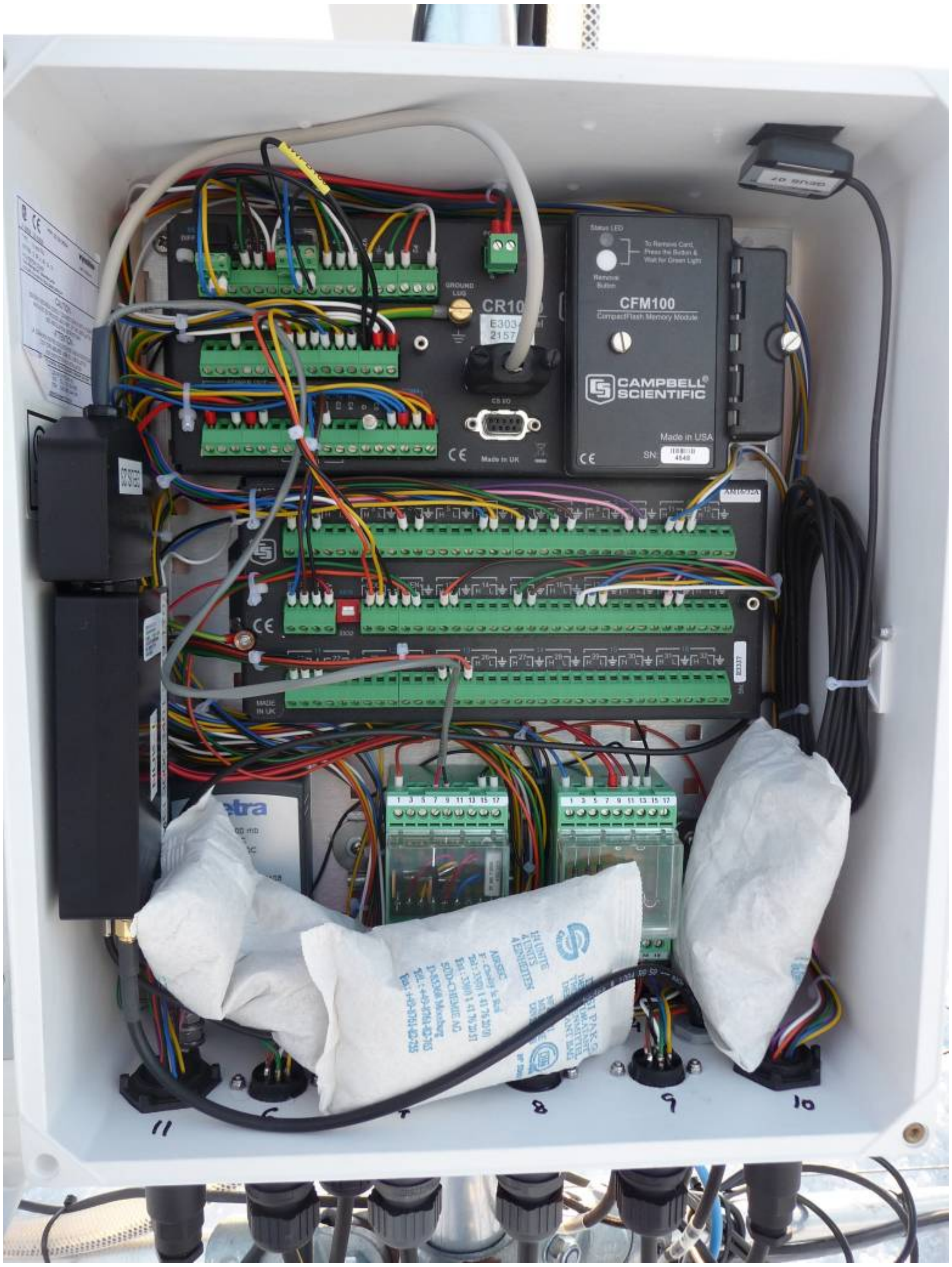

Figure 2. *A look inside a data logger enclosure. Some instruments, such as the GPS and the barometer are actually inside the enclosure. The white bags contain dessicant to remove humidity inside the box, which could otherwise cause problems with the electronics.*

1. Cut 10-string cable in 15 meter pieces.
2. Make 7-8 cm incisions where thermistors will be placed (8 in total, at 1, 2, 3, 4, 5, 6, 7 and 10 m depth), the 'lowest' at 10-20 cm from the end.
3. Cut the appropriate colored wire about halfway in each incision of the cable (orange, black, blue, yellow, green, brown, pink, violet). Cut away 'lower' part of the wire. The grey wire is not used, white is ground.
4. Remove 5-7 mm of coating from the end of the colored wires.
5. Remove about 1 cm of coating from the (uncut) white wire in every incision.
6. Place heat-shrinking tube around the loose end of a colored wire - this will prevent the two ends of the thermistor from touching. Don't shrink yet.
7. Twist one end of a thermistor around the bare end of a colored wire and solder it stuck.
8. Slide the heat-shrinking tube over the bare metal of the wire and thermistor and apply heat to fix it. Don't put too much heat on the thermistor itself!
9. Twist the other end of the thermistor around the uncoated part of the white wire and solder it to it.
10. Use some normal tape to prevent the thermistor from sticking out of the cable too much and getting damaged.
11. Repeat steps 6 to 10 for all incisions.
12. Make a mark for instance 20 cm next to each thermistor to be able to know their exact location after covering them up.
13. Cut heat-shrinking tube, diameter approx. 1 cm, in 15 cm pieces, one to cover every incision.
14. Slide these over the cable and fix partly directly over every incision by applying heat to one end. Shrink 2-3 cm. Be careful not to apply heat too long; this could damage the coating of the cable.
15. Prepare the glue. Don't touch, use gloves.
16. Fill the heat-shrinking tube with glue to 2-3 cm from the top using for instance a big syringe. Make sure no air is left inside.
17. Shrink the other end of the heat-shrinking tube. Glue might flow out and things will get messy.
18. Repeat steps 16 and 17 for the entire string, or do several thermistors simultaneously. You have 30-45 minutes before glue becomes inconveniently thick.
19. Leave thermistor string to dry for at least one night.
20. Determine the positions of the thermistors using the markings that you made.
21. Use these to determine where to place the piece of tape identifying the initial ice/snow surface during installation in the field (i.e. 1 meter above the first thermistor).
22. Put a 9-pole plug (preferably filled with silicone gel) on the top-end of the cable. Pin 1 = orange, 2 = black, ..., 8 = violet, 9 = white. No grey.
23. Place a piece of tape with the serial number of the thermistor string near the plug.
24. Close the bottom of the string using a heat-shrinking cap.
25. Attach ~4 cm cylindrical metal weight to the bottom of the string by filling it with silicone gel and pushing in the cable end. Let dry. Weight doesn't need to be too heavy.

Table 3. *Details of the thermistor string production.*

Before shipment, all sensors and other equipment for a station are mounted on a test tripod on the GEUS roof (see Figure 3). The new station is left running for a few days. If all systems are functional, the station is taken down and put in boxes for shipment to Greenland.

Figure 3. *Test tripod on the roof of GEUS.*

Database development

The purpose of the PROMICE database is to keep track of all data acquired in the PROMICE project, with what instruments they were acquired and what processing has been done to it. To begin with we will concentrate on data from the PROMICE stations. However over time it is the plan that other PROMICE data such as airborne altimetry data, radar surface velocity data and GLIMS glacier map data should be included.

There will be three types of users of the database: the GEUS glaciology group, the scientific community and for public outreach. It is a condition that data from the PROMICE project should be made publicly available. Therefore parts of the database will be accessible via internet. Initial planning of the PROMICE database development was carried out during 2007/08. The database will be a complex system including many different types of data and the development will have to proceed in phases.

The database will be developed as three separate units containing respectively station data, air borne altimetry data and satellite data. At a later stage it may be considered also to have a unit containing model results. The final quality-assured data will be available to researchers and the general public through the internet.

It has been decided to give highest priority to the development of the station data unit since this is the most demanding and highly in need unit. The station database will contain measurements, station information, instrument information and calibration information. Data quality assurance will be an integrated part of the system. The database will be organized in such a way that it can be used equally to access data, develop station maintenance plans and calibration plans. Finally it is also the plan to include data from complimentary stations funded by other sources such as from the projects FreshLink, SEDIMICE, Glacio-Basis, Greenland Analogue Project and others.

The database is being developed by the GEUS database group and will be stored in the GEUS data system which has been equipped with the presently required storage space and provides the possibility of expansions when necessary. Daily backups are run on the GEUS system.

Public access to the first consolidated PROMICE station data is expected by the end of 2009.

So far servers and storage have been purchased. A separate server will be installed for the access of data to the public and the scientific community via the internet. The database will be developed by the GEUS database group in close collaboration with the glaciology group and will be stored in the GEUS data system. For development of the PROMICE database we have selected ORACLE which is already used at GEUS. Programming of the data base is a demanding task which will proceed in 2009 together with running test data sets. Further development and refinement will be necessary in the following years.

The database system will be a complicated system containing several types of data. To ease the use and maintenance, interfaces to the database will be developed. This is being done by the database group with input from the glaciology group. Once the database interface is ready, the glaciology group members will be instructed in its use and if necessary adjustments will be made. It is the intention that most members of the glaciology group will be capable of using and maintaining the database.

The different types of data in the database need to be quality-assured. It is particularly important for the automatically collected station data to have standard quality assurance procedures. Therefore quality control will be an integrated part of the database and partly automatic. Consultations have been made with ASIAQ and DMI to learn from their experiences with weather station databases and quality control systems before designing the GEUS database as described below.

The data will be organized in a hierarchy where level 0 refers to the unprocessed raw data and meta data, level 1 refers to processed data and level 2 refers to time-averaged data. A flowchart of how the data will be organized and processed is shown in Figure 4.

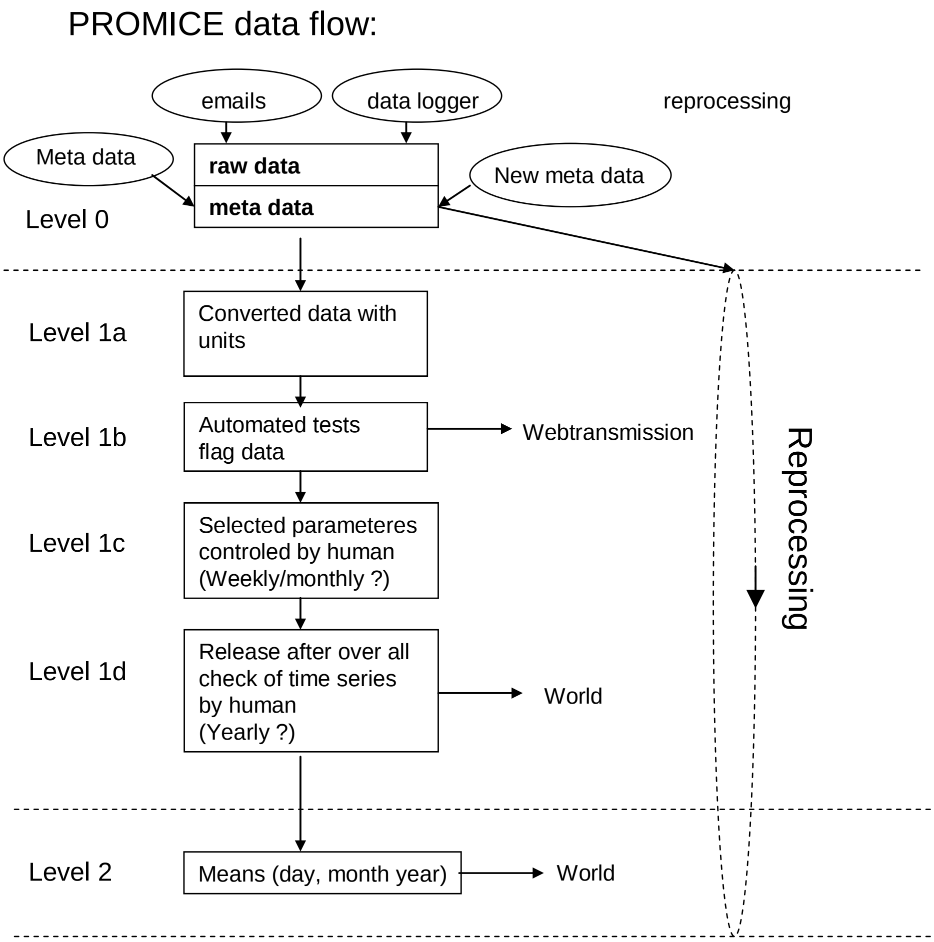

Figure 4. *Overview of the quality-assurance procedures for station data.*

The PROMICE station raw data consists of measurements from a number of instruments. Depending on the parameter/instrument the measurements consist of the actual physical quantity, a physical quantity which needs to be corrected or a voltage which needs to be converted into a physical quantity.

The measurements are sent to a data logger where they are stored and emailed to GEUS. Therefore two sets of raw data are produced in most cases. The transmitted data received at GEUS at near real time and the collected data stored in the data logger if it is retrieved from the station (if it is found and still working). Both data sets will be stored in the data base. A decision on which data set is of the highest quality and therefore should be the publicly available data set will be made. If collected data exists this is likely to be the best, since it will have the highest time resolution.

All meta data information on the station, instruments (type, serial number, accuracy, calibration, etc.) and conversion/correction factors should also be stored. This information should be updated as instruments are replaced/updated/calibrated or conversion factors change otherwise. Conversion/correction factors are needed to convert some parameters from level 0 to level 1 data.

Level 1

Level 1 data consists of actual physical quantities. Several steps are required before the level 1 data are in a quality controlled condition where we can make it publicly available. Each step will produce a further quality controlled data set which we will denote level 1a, 1b etc.

Level 1a: Conversion and correction factors are applied to convert measurements into physically meaningful quantities.

Level 1b: Automated tests are applied to either flag or remove bad data. Depending on the parameter following test may be performed: time check, limit check, step check, variability check, missing data check, consistency check, comparison with close lying stations. Level 1b data may be used for near real time web cast.

Level 1c: On a timely basis (e.g. once a week or month) a person will look at the data to catch any problems.

Level 1d: Once a year a person from the Glaciology Group will perform an overall check of the time series of data. If the quality of the data is acceptable it is made publicly available.

Level 2

Time averaged data (day, month year) from the level 1d data is made publicly available. Statistics on the number of data points used in the averaging will be included.

Reprocessing

If e.g. conversion factors change at a later stage it may be necessary to reprocess the dataset by going through level 1 and level 2 again.

Development of the ablation assembly

The GEUS ablation assembly chiefly consists of a 25-50 m long liquid-filled hose and a pressure transducer which is located at the end/bottom of the hose. The sensor cable runs through the hose until it exits through a water-tight connection and is connected to the data logger of the automatic weather station. A liquid-filled bladder of a few liters at the start/top of the hose makes sure that volume changes in the liquid or the hose itself, by solar heating for instance, does not lead to an unrealistic increase in pressure in the assembly (see Figure 5). The hose is drilled into the ice up to 40 m depth. The pressure signal recorded by the pressure transducer deep in the ice is that of the vertical column of liquid over the sensor. This signal can be translated into depth knowing the density of the liquid in the hose.

As, over the years, the ablation assembly melts out of the ice (if installed in the ablation zone), an increasingly large part of the hose will be found on the ice surface, and the vertical column of liquid in the hose will get smaller. This reduction in pressure gives us the amount of ice that has melted away over the period.

By measuring at (sub-)daily timescales this assembly is well-suited to monitor ice ablation in remote regions, with clear advantages over other well-established methods of measuring ice ablation in the field. For instance, stake readings provide accurate information on surface height change, but form a low-frequency record as readings can only be done when the stakes are visited. Sonic ranger observations do give a continuous record of surface height, but the quality of the readings from these sensors reduces in time as they degrade due to continuous cycles of moisture freezing on and melting off them. A larger problem is that sonic ranger need to be mounted on stake assemblies drilled into the ice. After a single year of melt these stake assemblies can be melted out as much as six meters, often causing them to collapse during strong wind events. In theory, the pressure transducer ablation assembly can measure at high frequency, and keep on doing so until it has melted out of the ice – which can in theory be over ten years.

Figure 5. *The liquid-filled bladder at the top of the hose is housed in its own enclosure to protect the system from the harsh climate.*

The first deployment of a pressure transducer assemblies aimed at measuring ice ablation, was in 2001 and 2002 on the Qassimiut lobe, in southern Greenland. This region is characterized by extreme surface melt values in respect to most other locations on the Greenland ice sheet. Figure 6 shows the ablation record as obtained by pressure transducers between 2001 and 2007. Negative values indicate the amount of glacier ice that has ablated within a year. Positive values indicate the presence of a snow layer that has accumulated over the previous winter. Yearly net ablation values range from 5 to 6 m of ice.

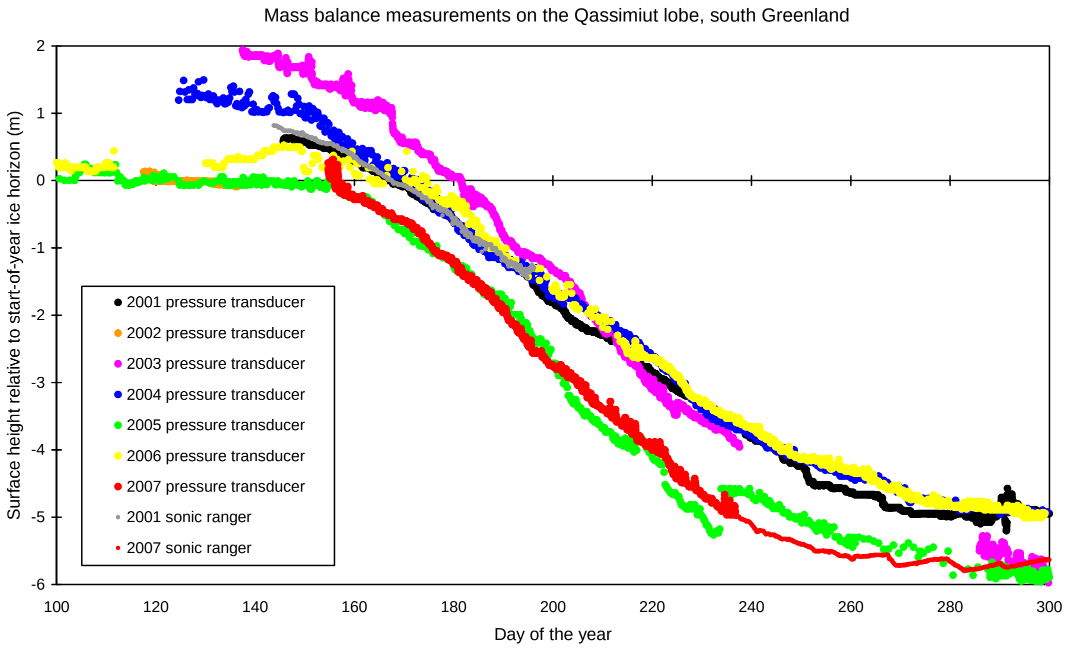

Figure 6. *Melt records obtained with the pressure-transducer system (fat lines) compared with a few records from the sonic ranging system (thin lines) on the ice sheet margin by Sermilik Bræ, near Qassimiut in South Greenland.*

A few years later more pressure transducers were installed on the Greenland ice sheet: three in the Nuuk region in 2003, two in the Tasiilaq region in 2004, and one in the Melville Bay region in northwest Greenland in 2004. Even though the first results were promising and showed that the idea had potential as seen in Figure 6, a few issues had to be dealt with in the development of the assembly. Here we will list the issues and changes that have been implemented over the past years.

Pre-PROMICE improvements

- Originally, the liquid used in the assembly was pure alcohol. Besides the problems this created with the customs when shipping to Greenland, there were occasions that upon return to the automatic weather stations, the alcohol had largely escaped the assembly due to reasons unknown. The alcohol was replaced by a 50/50 antifreeze and water mixture, which can be bought anywhere and shipped without problems.

- Another improvement concerned the bladder, which used to be laying on the surface, allowing it to move around and be covered by snow in winter. The bladder was tied to one of the legs of the tripod of the automatic weather station to keep it in place, and protect it from the elements to a certain extent.

- Finally, the diameter of the hose used in the assembly was increased from roughly 1 cm to 2 cm to keep the hose from being pressed closed by the pressure of the ice.

PROMICE improvements

- During PROMICE, we made the pressure transducer system shorter, for easier shipment, easier handling (less space and weight in the helicopter), and to prevent an assembly to remain in the ice for more than a few years (which would make it impossible to recalibrate them in accordance to the calibration plan). The current hoses are 25 m long, and are drilled roughly 20 m into the ice, which should be sufficient to monitor ice ablation for at least four years.

- The previous pressure transducers required an open connection to the atmosphere, to be able to measure the pressure of the vertical liquid column in respect to the local air pressure. This required a second thin tube to run from the sensor to the surface. To avoid closure of this delicate second tube, and to simplify the assembly all together, we started using absolute pressure transducer, which do not require an open-air connection.

- Possibly the most important change is that the bladder of the assembly is no longer tied to one of the legs of the tripod, but is placed in an enclosure on the main mast. By keeping the bladder in an enclosure, it is much better protected from the elements and leaks should occur less often. By having the bladder on the main mast instead of a leg of the tripod, the unavoidably tilt of an automatic weather station in the ablation zone will result in less of a vertical change in position of the bladder, thus increasing or decreasing the length of the vertical liquid column.

The fact that PROMICE automatic weather stations are equipped with both a pressure transducer and two sonic rangers, allows us to validate the output of the former sensor. Current results show that some PROMICE pressure transducers show a fairly large and unexplained variability, but overall we have improved the system considerably since the early test in 2001. The data of the current stations will help us to assess any further issues with the pressure transducer system and improve the system further.

Development of data transmission by satellite

Telemetry from the AWS's in the field to GEUS answers four major requirements of the PROMICE monitoring programme:

1) Reliably provide early observational data for science use
2) Secure the availability of field data even in case the station disappears
3) Assist in maintaining the observation network operational while minimizing the frequency of expensive site revisits

4) Satisfy requirements 1 and 2 at an affordable cost

Ideally, one single communication solution should suit all of the planned sites, to allow a standardized design of the stations.

Ground-based radio-modem transmission has been ruled out based on cost and technical issues, since the remote location of most sites would require either intermediate radio repeaters (involving expensive field maintenance) or powerful transmitters consuming more supply power than available. This leaves only satellite-based telemetry as an option, and previous experience both within and outside GEUS support this choice.

During the late 1990's and early 2000's several commercial operators of satellite telecommunication services faced serious financial difficulties or even faced bankruptcy. Given the considerable investment in dedicated equipment and design effort to integrate a specific telemetry solution into the AWS design, the outlook for future availability of the service has been taken into account.

Several satellite systems are in use within the glaciological community for transmitting ground observations from remote locations. The AWS's of the Greenland Climate Network (GC-Net) operated by the University of Colorado at Boulder use the GOES Data Collection System (DCS) south of 72 N and ARGOS DCS north of 72 N. The ARGOS DCS system is also used by AWS's operated by the Institute for Marine and Atmospheric Research, Utrecht University (IMAU) both in Greenland and Antarctica, as well as by several other Institutions. More recently, applications based on the Iridium satellite constellation are also being introduced. The existing GEUS stations have been using the Inmarsat system of geostationary satellites, and further details about its performance, as well as the rationale for switching to a better option, are discussed below.

The GOES DCS is a relay system where synchronized AWS's on the ground transmit to one of the two geostationary GOES satellites within preassigned wavelength and time slots. The satellites retransmit the message to a ground station but the one-way nature of the communication doesn't provide any acknowledgment of successful transmission. The GOES DCS is technically unsuitable for PROMICE because the coverage is limited to latitudes south of 72 N. In addition to this, achieving high reliability would be difficult due to the lack of acknowledgment of successful transmission and to the requirement of maintaining a comparatively tight synchronization to transmit during the predefined time slot allocated to each AWS. Furthermore, direct access to the system is only available to U.S. federal, state, and local government agencies, and a U.S. government sponsor is otherwise required.

The Argos DCS is another one-way data collection relay system that adds the benefits of providing global coverage and platform location. The AWS's on the ground transmit to the Argos instrument aboard the NOAA Polar-orbiting Operational Environmental Satellites (POES), but no acknowledgment of successful transmission is available in the original Argos system (it is currently being implemented in Argos-3 instruments). The data rate is still limited, and new terminal devices able to implement the full Argos-3 have only started being introduced in late 2007, therefore Argos has not been selected for use in the PROMICE AWS.

The existing GEUS pre-PROMICE AWS design used a Thrane & Thrane A/S device to transmit data through the Inmarsat satellite newtork. Due to the geostationary orbit of the Inmarsat satellites, their coverage is generally specified as limited to 82 N, and local topography and environmental conditions may make service availability marginal at high latitudes (see Figure 7). This setup suffered from some shortcomings:

- Marginal radio performance due to the low elevation of the geostationary satellite over the horizon
- Unsuitable for the northernmost planned AWS sites
- Low reliability with several lost transmissions
- No wintertime transmission for power consumption considerations

Because of these limitations, it was decided to switch for a better suited satellite telemetry system not based on geostationary satellites.

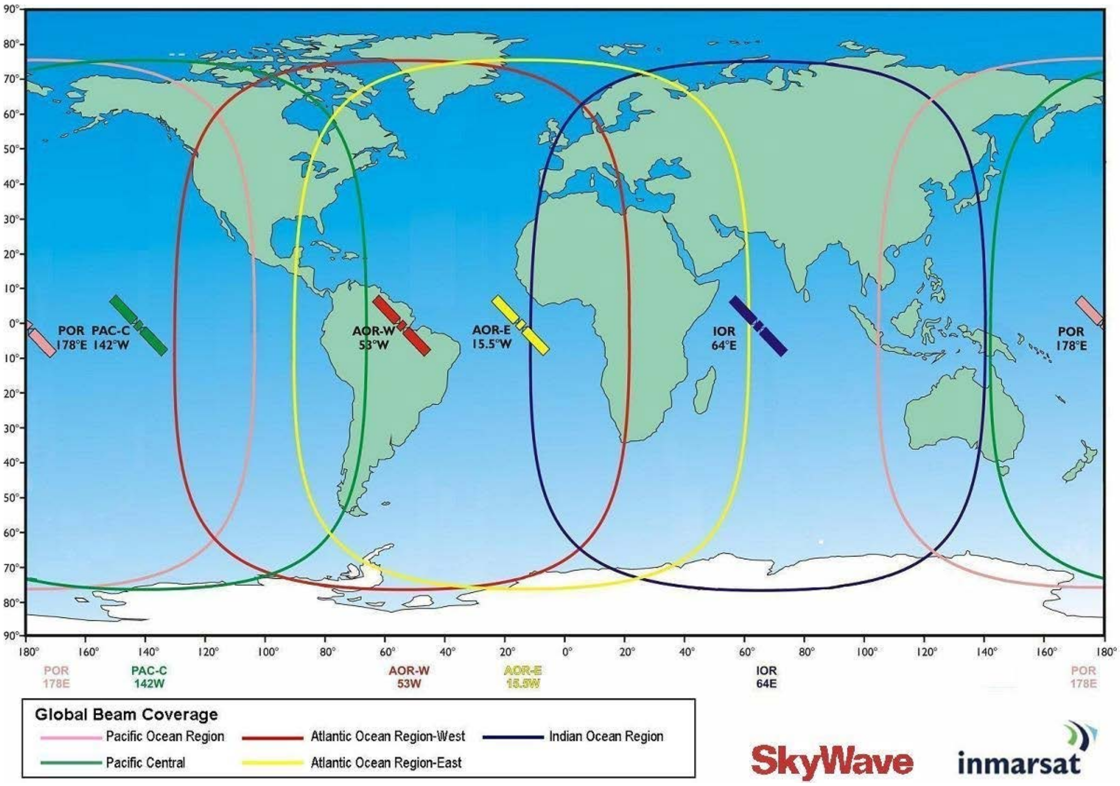

Figure 7. *Radio footprint of the Inmarsat geostationary satellites used by GEUS' existing pre-PROMICE AWS's. The coverage at high latitudes is marginal.*

Iridium, GlobalStar and ORBCOMM are the three major operators but only Iridium satisfies all PROMICE requirements, in particular concerning to good coverage at high latitudes. Due to their orbital configurations both and provide limited (GlobalStar) or no coverage (ORBCOMM) (Figure 8). The Iridium satellite constellation is based on 66 active satellites in low Earth orbit (LEO) at a height of approximately 781 km and inclination of 86.4°, with several in-orbit spares. Coverage of polar regions is therefore optimal (Figure 9), and data transmission service and equipment are readily available commercially. The initial financial difficulties experienced by the Iridium commercial operator have been overcome and the outlook for continued reliable service has been considered good, based on the reported growing number of subscribers and extensive use by the U.S. Department of Defence. Iridium has therefore been chosen as the satellite telemetry system used by PROMICE AWS's.

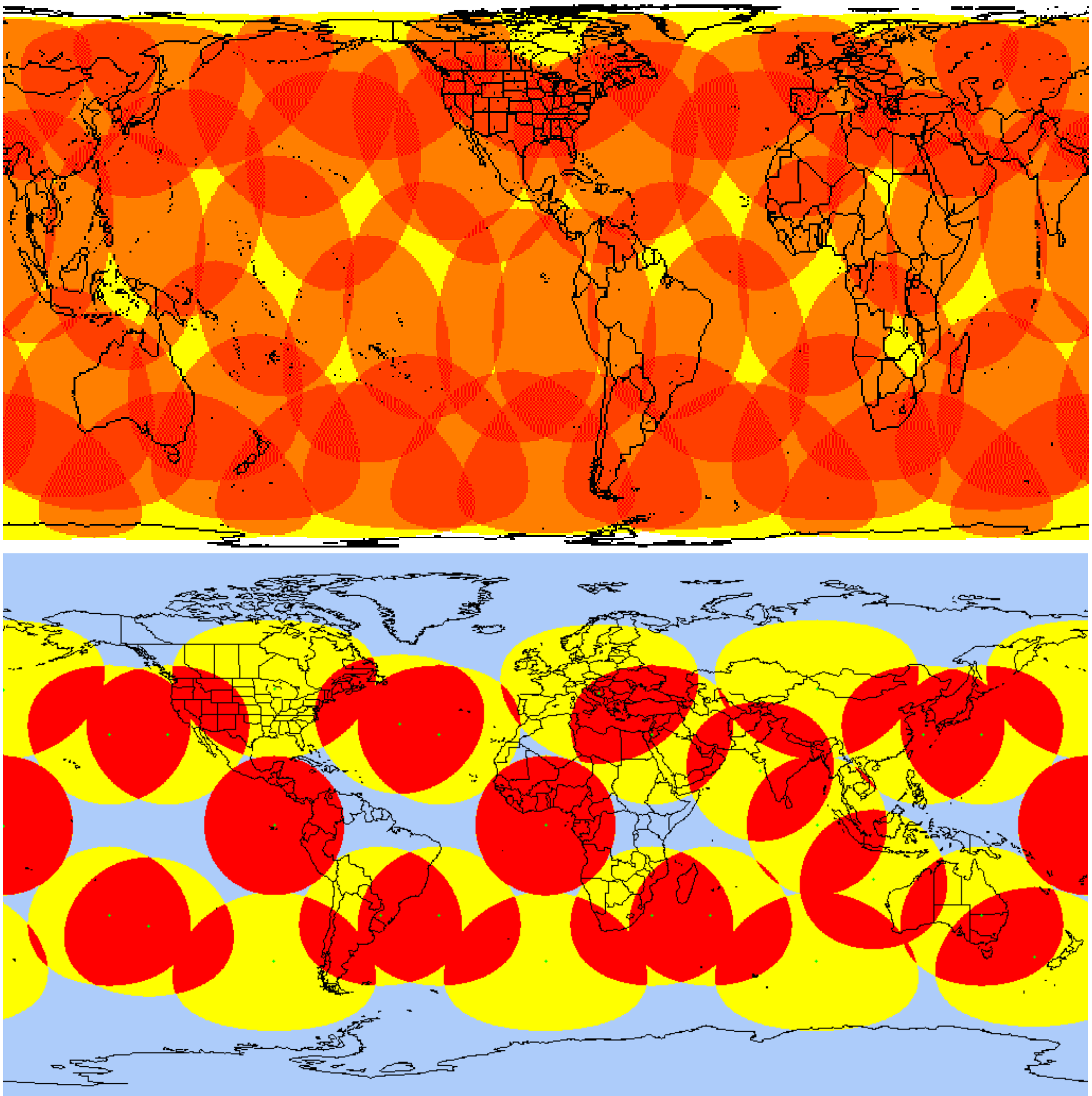

Figure 8. *Snapshot radio footprint of the GlobalStar (above) and ORBCOMM (below) satellite constellations. Since the satellites are in LEO polar orbits, the footprint of each satellite changes rapidly over time, however the system coverage remains comparable and limited (GlobalStar) or absent (ORBCOMM) over polar regions (yellow: one satellite in view; darker shades of orange and red: two or more satellites in view).*

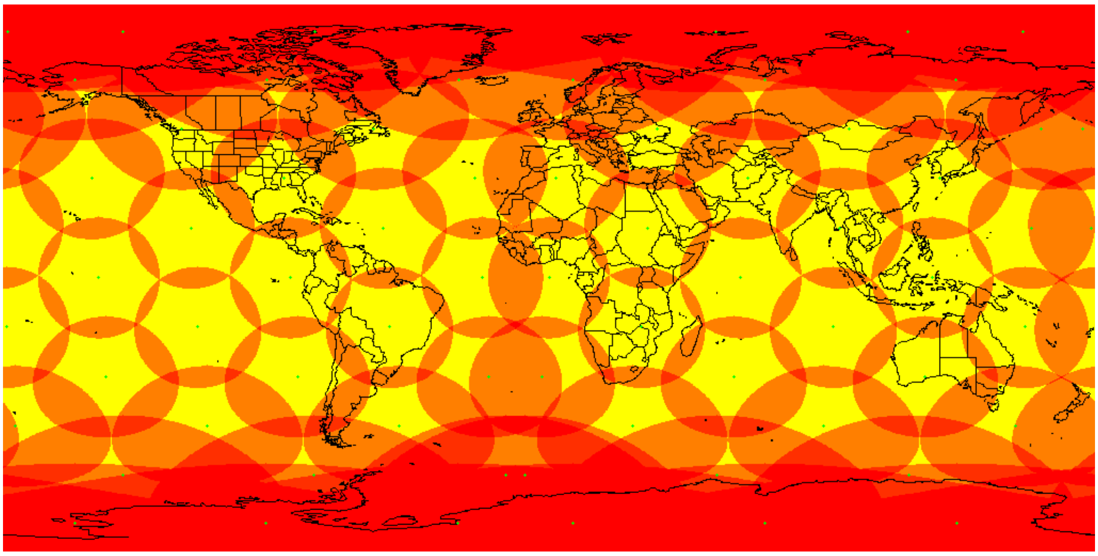

Figure 9. *A snapshot radio footprint of the Iridium satellite constellation. Since the satellites are in LEO polar orbits, the footprint of each satellites changes rapidly over time, however the system coverage remains comparable and very dense over polar regions (yellow: one satellite in view; orange: two satellites in view, red: 3 or more satellites in view).*

A particularly interesting operational mode called SBD (short burst of data) is offered at an affordable price, and specialized data terminals are commercially available. The cost analysis including various billing options is described in the following section based on rates in USD from early 2008.

Data transmission cost analysis

The cost of Iridium airtime has been determined in relation to the fees levied in early 2008 by NAL Research Corp. Two types of service contracts are offered: a “standard” and a “fixed” rate contract. For the anticipated volume of traffic generated by this application, the “fixed” rate is the cheapest option both at the wintertime and summertime transmission rates (Figure 10). A check has been done with the actual costs invoiced by NAL for one entire month showing the estimates below to be accurate.

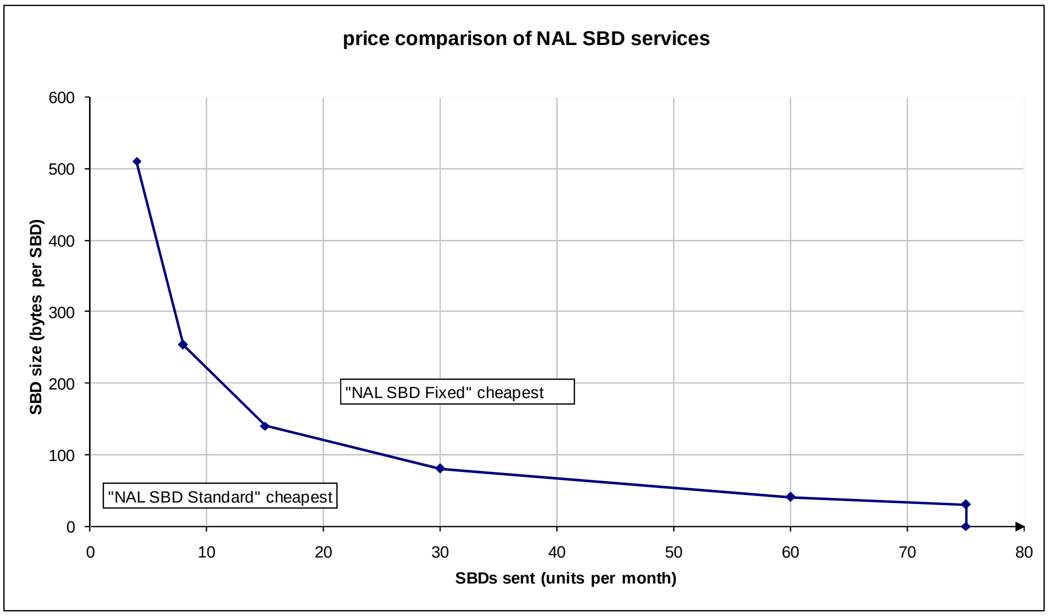

Figure 10. *Plot comparing the "fixed rate" and the "standard rate" fees offered by NAL Research Corp. for Iridium SBD airtime.*

Figure 11. *Monthly price of SBD airtime at summertime transmission rates.*

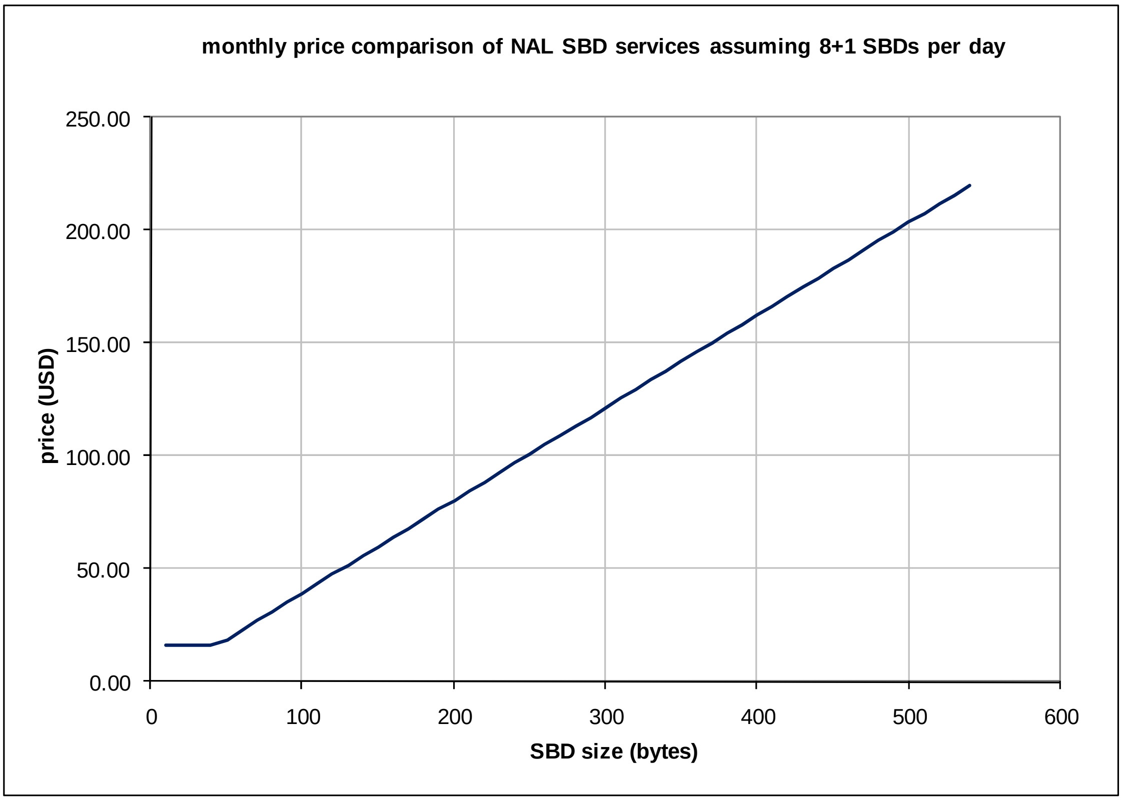

Figure 12. *Monthly price of SBD airtime at wintertime transmission rates.*

The summertime estimated monthly cost of Iridium SBD airtime, based on a volume of traffic of 760 SBD messages per month (also including the diagnostic messages) and an average size of 300 bytes per SBD message corresponds to about 340 USD (Figure 11). The entire April to October season will cost 2380 USD. The wintertime estimated monthly cost of Iridium SBD airtime, based on a volume of traffic of 275 SBD messages per month (also including the diagnostic messages) and an average size of 300 bytes per SBD message corresponds to about 120 USD (Figure 12). The entire November to March season will therefore cost approximately 600 USD.

The cost of Iridium SBD airtime for an entire year will therefore amount to about 3000 USD, which fits within the anticipated budget. This expense could be significantly reduced by modifying the program so that it encodes the data in a binary format before transmission.

Hardware and software implementation

The Iridium SBD transceiver model 9601-DG manufactured by NAL Research Corporation has been selected as it offers two-ways SBD communication and integrated GPS positioning in a rugged device specified for operations within the temperature range -30 to 60 °C (storage -40 to +85 °C) and certified to military standards for thermal and mechanical shocks, humidity and vibrations. The unit requires sufficiently low power that transmissions can be extended to cover the entire winter season. This is a particularly important advantage over the previous system because several stations in the past operated and transmitted properly until transmissions were suspended for the winter and then never resumed transmitting in the spring, thus providing no clue about what kind of failure might have occurred and what field maintenance would have been required.

The required code was integrated in the new datalogger program developed for the Campbell Scientific CR1000 dataloggers included in the new AWS design.

Power supply and data connection to the NAL 9601-DG is through a NAL SYN-DC-936 DC-DC power converter efficiently lowering the 12 V battery supply to the required 5 V. The datalogger controls the 12V supply to the NAL SYN-DC-936 through a solid state relais, only activating the supply at times scheduled to acquire reliable GPS fixes or to transmit data messages. The datalogger communicates to the NAL 9601-DG over an RS-232 serial link passing through the NAL SYN-DC-936, and every unit requires that the male 9 pins D-type connector supplied by NAL be replaced with a female 9 pins D-type connector matching the connector in the CR1000 datalogger. It is also required to rewire the connector pins because the transceiver expects to be attached to an RS-232 DTE (data terminal equipment) device but the CR1000 connector is wired as a DCE (data communication equipment) device. The transceiver is housed within the logger enclosure and connection to the antenna mounted on top of the mast is through an RG58 coaxial cable.

Transmission is currently encoded as printable ASCII and Figure 13 shows an example message as received from a PROMICE AWS in the field. As a future improvement it is being considered to switch from ASCII to binary encoding, which would reduce the amount of bytes transmitted by about 50%, with a corresponding cost reduction. The transmitted data messages are automatically sent to GEUS as email attachments.

```
2008-09-06
01:00:00,360060,912,1.93,41.56,99.4,1.581,264.1,10.13,0.221,
-0.331,0.433,-4.745,1.712,2.858,0.826,13.09,-0.528,-1.726,-2.751,-
3.59,
-4.199,-4.584,-4.725,-4.525,-
0.37,2.195,010014.60,6705.83936,04955.91265,
671.4,0.94,123.3,12.81,!S,!M
```

Figure 13. *An example of a message from the PROMICE AWS at 300034012250840.*

The logger program implements several configurable functionalities aimed at increasing the reliability of the telemetry and at the same time reducing power consumption. The program can switch on the NAL 9601-DG at predefined intervals independently either for obtaining a GPS fix, for transmitting tasks or for both tasks at the same time, in every case supplying power only for the shortest time needed. This is important because the GPS needs some time to produce a reliable fix, but this is not necessary at times when only transmission has to be performed. The logger program also uses the available power management commands to selectively switch on and off the internal components of the NAL 9601-DG (i.e. GPS module, control interface, and RF section).

When transmission is to be performed, the logger uploads the message to the NAL 9601-DG, activates the RF section and waits for confirmation that an Iridium satellite is in view before trying to transmit the message. If, for any reason, no satellite is found within a short predefined timeout, the logger switches off the transceiver and queues the message that failed to be transmitted in a first-in first-out queue implemented in the logger program. This is necessary in spite of the good Iridium coverage of the polar region to prevent a faulty transceiver, coaxial cable or antenna from wasting battery power by waiting too long or by transmitting "in the blind". If, as normally is the case, a satellite is detected and signal strength is good, transmission is attempted. In case of transmission failure, as indicated by the return codes issued by the NAL 9601-DG, the logger will check that the satellite is still in view and then try again to transmit the message until transmission is successful or until the predefined timeout is reached, after which the transceiver is powered down. In any case, all messages that could not be sent will be queued in the FIFO. The queued messages will then be sent at the next scheduled transmission, if possible, or kept in the queue for further attempts until they are transmitted successfully or the FIFO is full, after which the oldest unsent messages will be dropped. This system allowed obtaining 100% transmission reliability in the AWS's deployed to date.

Both GPS and transmission intervals can be configured in the logger program at different rates for summer and winter, in order to save costs and battery power during wintertime. As a further safety, the datalogger monitors the battery voltage and stops using the GPS and Iridium transceiver if the battery voltage drops below a predefined low-battery threshold. A configurable hysteresis prevents instability and erratic behavior by resuming full operation only after the battery has been charged by the solar panels to a voltage higher then low-battery threshold. This system makes much better use of the available batteries by allowing to wire them as one single large battery array in place of the commonly adopted scheme of wiring two separate arrays dedicated one to the datalogger and the other to the satellite transmission.

Placing transects of automatic weather stations on the ice sheet

There are currently six PROMICE automatic weather station transects in Greenland. In 2010 the seventh transect will be placed to complete the PROMICE network. Each transect consist of two AWSs; one near the equilibrium line where yearly accumulation and ablation are balanced, and one at low elevation well into the ablation zone. (NB: The TAS-transect in the southeast / Tasiilaq region is the exception, where both stations are positioned at low elevation). A map of the currently active automatic weather stations (and a few prior stations) placed on ice in Greenland is shown in Figure 14, including US and Durch stations, as well as Danish (GEUS) stations not related to PROMICE.

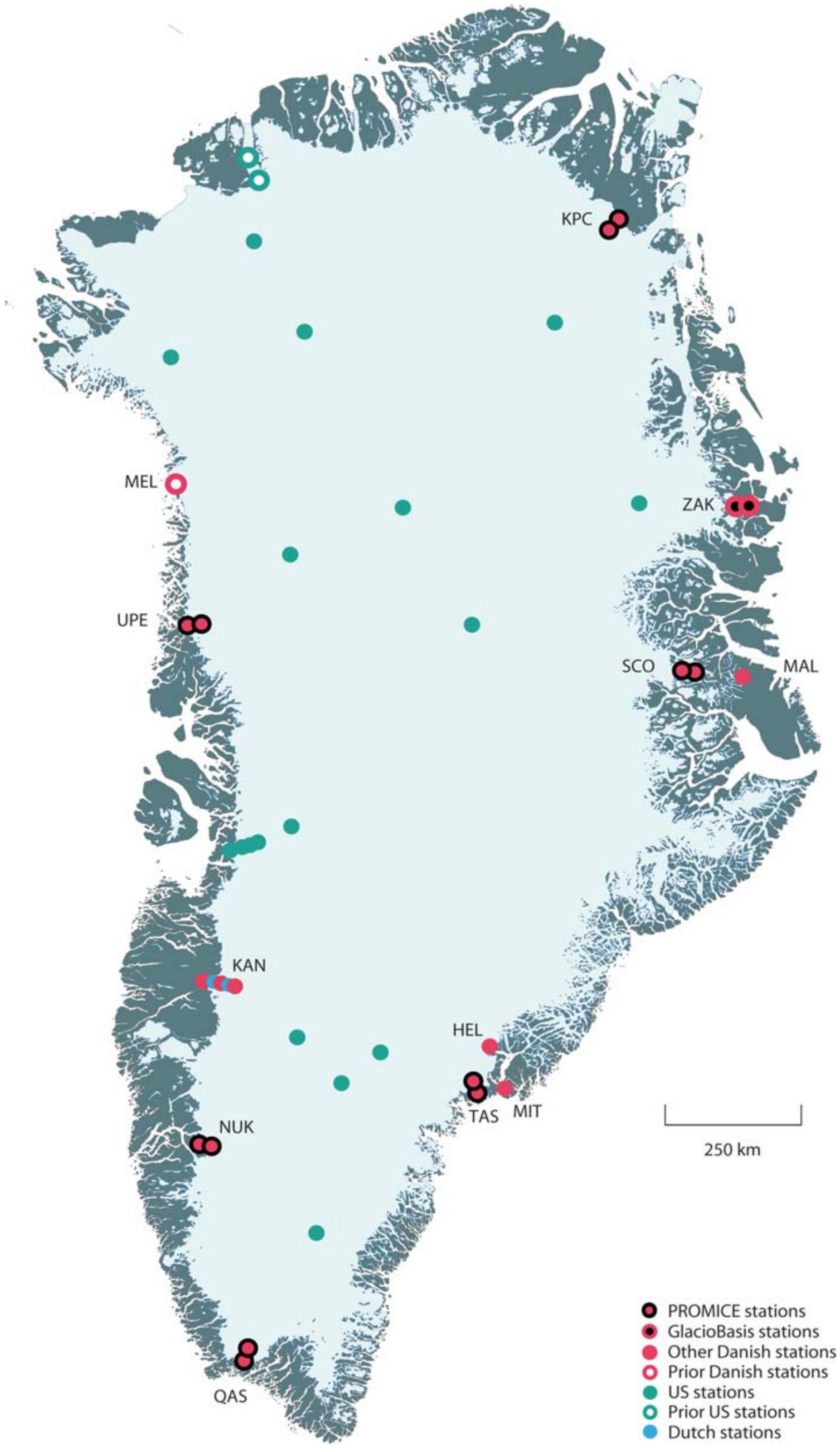

Figure 14. *Map of currently active automatic weather stations on ice in Greenland plus a few prior stations. The stations marked MIT and MAL are placed on local glaciers, the rest are placed on the Greenland ice sheet proper. Prior stations (marked with a white central dot) have been removed but are shown for the sake of completeness. Some prior US stations may have been omitted. The UPE transect was added in 2009.*

The initial construction of all AWS transects is/was done by helicopter. This means of transportation allows us to bring more weight to the ice than the alternatives offer, albeit at much higher cost. Unless the situation requires a different approach, we start constructing the upper AWS, as the weather is less predictable the higher you travel onto the ice sheet. Placement of a single AWS takes about three hours depending on the level of preparation done before going to the ice. A way to shorten the stay on the ice is to construct the entire aluminum tripod prior to the helicopter charter, which involves attaching wires, shackles, kee clamps, feet, etc., and folding it to be able to fit it into the helicopter. Also, the boom holding most of the sensors can be prepared off the ice, provided the sensors on the boom will be wrapped before shipment to avoid damage. Major advantage in this is that the sensors need to be aligned carefully (within half a degree), for which you need to take time and which is easier in a warm environment.

The placement of an AWS starts with unfolding the tripod, tightening the steel wires, and laying it on its side using a custom-made rest (see Figure 14). The boom with sensors are mounted at the top of the mast, and below we mount the temperature and humidity assembly, the solar panel, the enclosure of the pressure transducer assembly, and the logger enclosure. All cables are plugged into the logger enclosure and tied to the mast. After putting the tripod on its feet, we carefully orientate the station so that the boom is exactly in north-south direction, with the radiation sensor directed towards the south, and the wind speed sensor towards the north. Also, the solar panel is mounted facing south – so that at the end of the dark winter during which the station has been using up part of its power reserve, the batteries can be recharged as soon as the sun rises for the first time in the year. After orientating the station correctly, the battery box is hung underneath the tripod with a set of wires, and the station is powered up. The weight of the battery box (about 50 kg) functions as an anchor in that it keeps the station upright during strong winds.

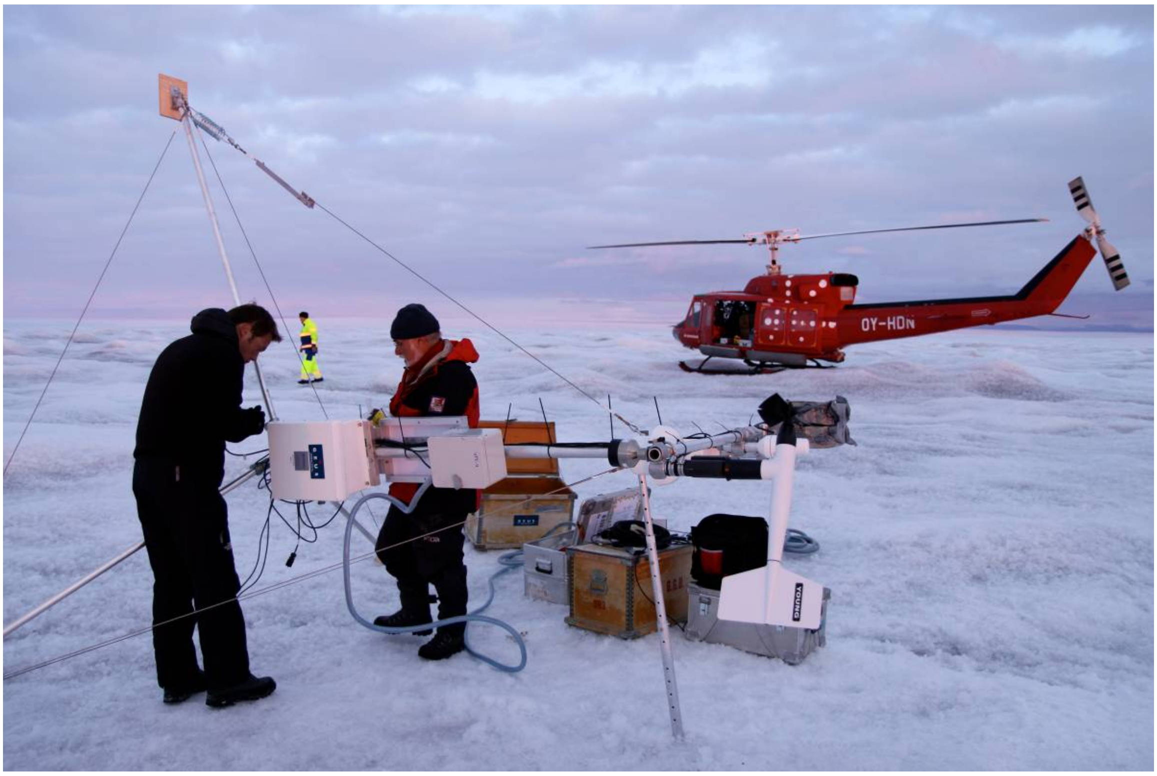

Figure 15. *Mounting of instruments and boom on a station tripod on the ice sheet. Note the practical, adjustable custom-made rest.*

Three sensors are not (fully) mounted on the AWS: the pressure transducer assembly, the thermistor string, and the second of the sonic rangers. The holes for the pressure transducer and thermistor string are drilled into the ice using either a mechanical Kovacs drill (faster and lighter), or a steam drill (more reliable). The second sonic ranger is mounted on a stake assembly consisting of three interconnected stakes, which is also drilled into the ice. All drill holes combined add up to a length of roughly 50 meters.

Figure 16. *Drilling with the Kovacs mechanical drill. Note the practical one metre auger pieces.*

With all sensors mounted and the system powered up, the station is operational. We test the AWS by connecting a laptop to the logger. With this we read out the current values that the sensors measure, including for instance GPS position and the currant of the fan ventilating the temperature and humidity assembly. If a value is out of its normal range, we look into the problem.

Finally, we fill in a check list, which give us crucial information on position, initial station tilt, length of the stakes at installation, anything out of the ordinary, anything we may have forgotten, etc. After this, we pack everything in the helicopter and clean up behind us before we move to the second location to place the other AWS.

Performing maintenance on transects of automatic weather stations

Visiting an existing (transect of) automatic weather station(s) is commonly done by helicopter – as is the initial installation. However, two (or three depending on the location of the final transect in 2010) transects have been placed in regions where we can get to over land. For the stations in the northeast (the KPC transect in Figure 14) the use of snow mobiles allows us to visit the stations from Station Nord in spring. For the stations in the southeast (the TAS transect in Figure 14) we have connections with the inhabitants of Tasiilaq and surroundings, who assist us in travelling to the stations by dog sled (See Figure 17).

Figure 17. *Visiting the station transect near Tasiilaq in Southeast Greenland by dog sleds.*

There are several levels of thoroughness in performing automatic weather station maintenance. The lowest level for a station visit occurs when someone unfamiliar with the system is visiting a station. We ask this person to either download the data or replace the memory card in the logger enclosure so we obtain the full data record. In addition, the person is asked to fill in a checklist and make photos so we learn of the current status of the station.

The next level of thoroughness is when GEUS personnel familiar with the station design visit a station. For a station that is fully functional, standing upright and orientated correctly, we perform the actions as described above, and replace the hygroclip (humidity and temperature) and the membranes in the sonic rangers. If needed, we upload a new program into the logger. A station visit of this type takes 30-45 minutes, which is how long it takes to download one year worth of data onto a laptop. Depending on the ablation rate at the station we may have to drill new holes for the stake assembly and/or thermistor string and/or pressure transducer, which will add to the time spent at the station considerably.

If some sensors are malfunctioning or the tripod is not positioned as it should, attending to this will take up a lot of time (2-6 hours depending on the damage). Problems can range from sensors destroyed by strong winds, to having melt water in the system, to bent tripod legs, to stations on their sides because of extreme winds or crevasses (See Figure 18). If a station is visited in spring (See Figure 19), a snow layer of up to two meters will complicate work on the station – digging through such a layer of snow will take hours alone. For a particular visit at the lower TAS station in Spring 2009, removing the snow from the (toppled) station took six hours with six men working in shifts of three.

In our experience, replacing an old station by a completely new one takes less time than doing a considerable amount of maintenance work on a station, i.e. replacing parts and sensors. This has to do with the fact that building and taking down stations are straightforward activities, while doing repairs on a station could involve all sorts of surprises.

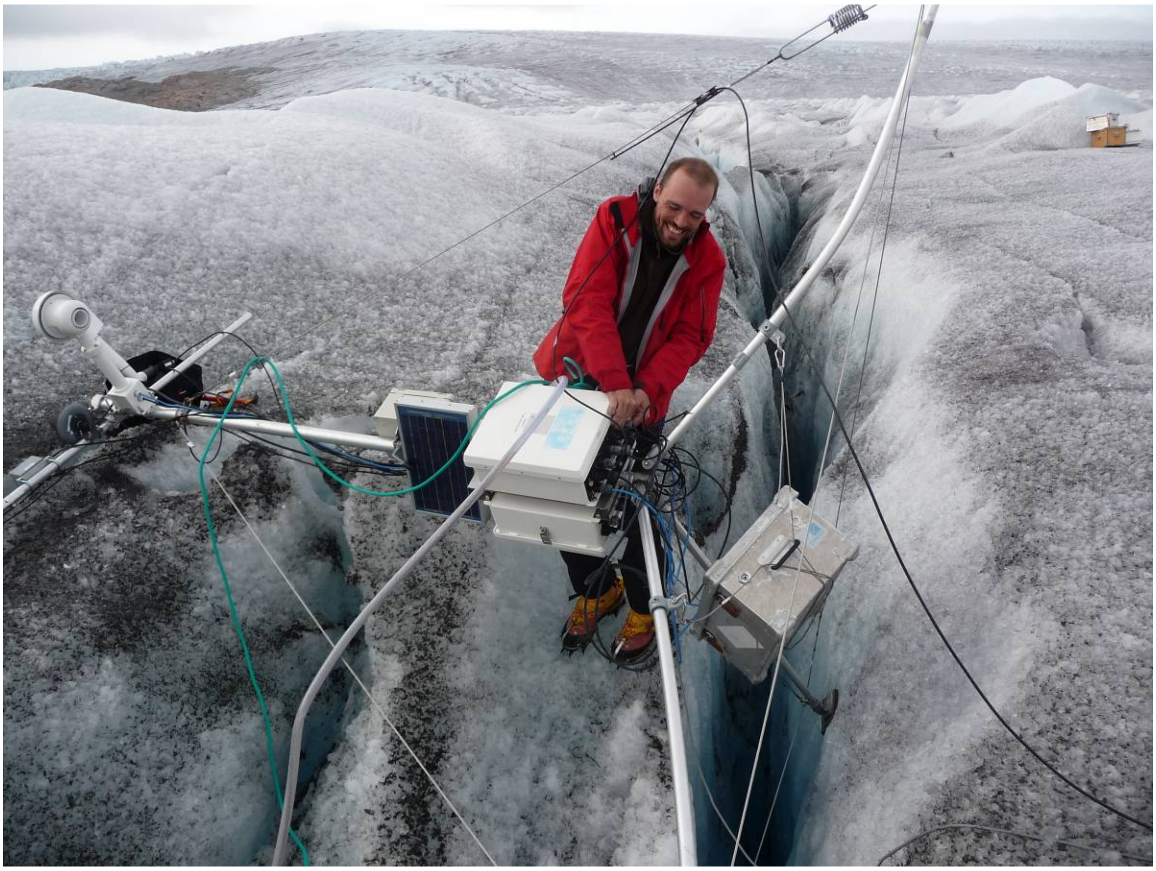

Figure 18. *Salvaging instruments from a station fallen into a crevasse on the Qassimiut lobe in South Greenland.*

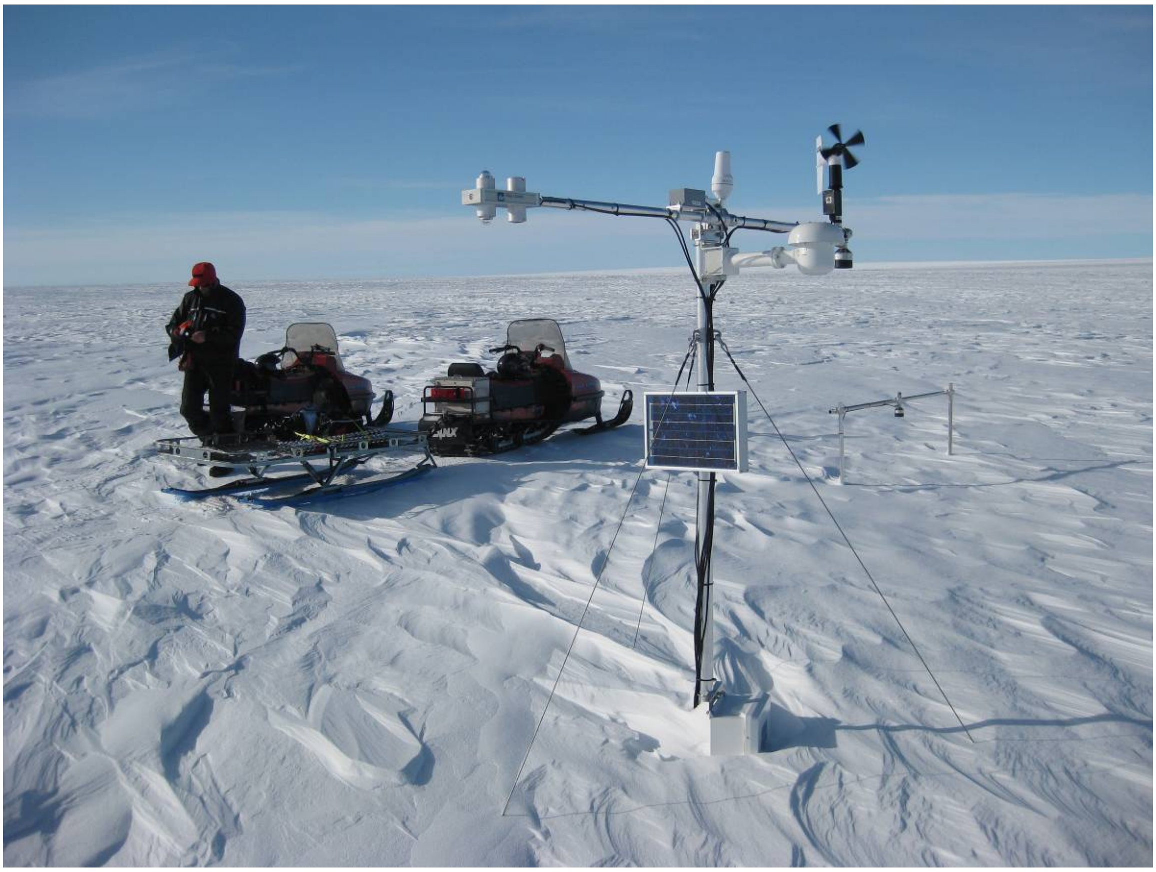

Figure 19. *A station in springtime covered in snow.*

Data treatment and success rate

Station description

We are working towards having a network of 14 identical automatic weather stations (AWSs) within PROMICE. For various reasons the AWSs and their logger programs underwent a few changes since the start of the programme in 2007. The text in this chapter deals with the latest assemblies of hardware and software versions: the PROMICE 2008/2009 station design, and the 2009 logger program.

The PROMICE AWSs are equipped with:

- a CR1000 data logger and AM 16-32A Multiplexer
- a NAL 9601-D Iridium transmission system with GPS antenna
- a Campbell CS100 barometric pressure sensor
- a ventilated Rotronics radiation shield holding a MP100 temperature probe and a HygroClip temperature & relative humidity sensor
- a Young 05103 wind monitor
- a Kipp & Zonen CNR1 net radiometer
- two Campbell SR50 sonic rangers (one on the AWS, one on stakes)

- one GEUS-made ablation assembly using a NT1400 pressure transducer
- a GEUS-made thermistor string with eight PT100 thermistors
- a NS25-E2 tilt sensor
- a BP Solar 10-Watt solar panel
- four Panasonic 28 Ah sealed lead-acid batteries

AWS output

Measurement and transmission frequencies

The PROMICE AWSs measure and store data every ten minutes. The only exception to this are the wind speed observations, which give the mean wind speed since the last measurement cycle, and the GPS measurements, which follow the transmission schedule. In winter (days of year 300 to 100), values of measured quantities are transmitted just once a day – to limit power consumption when solar power is not available – at midnight. In summer (days of year 100 to 300), values are transmitted on the hour, every hour. The transmissions consist of average values (daily or hourly) of the more variable quantities, such as temperature and radiation. Instantaneous values of less variable quantities, such as surface height and station tilt, are appended once every six hours in summer, and every day (thus for all transmissions) in winter.

Column assignment of raw data files

<u>Locally stored logger data</u>

1- Date and time (UTC)
2- Record number
3- Minutes in year
4- Air pressure (hPa)
5- Air temperature by PT100 (°C)
6- Air temperature by HygroClip (°C)
7- Relative humidity (% with respect to water, not ice)
8- Wind speed (m/s)
9- Wind direction (° relative to north at installation)
10- Wind direction standard deviation
11- Incoming shortwave radiation (~V)
12- Outgoing shortwave radiation (~V)
13- Incoming longwave radiation (~V)
14- Outgoing longwave radiation (~V)
15- CNR1 casing temperature (°C)
16- Snow height by SR50 on AWS (m)
17- Snow height SR50 measurement quality
18- Surface height by SR50 on stakes (m)
19- Surface height SR50 measurement quality
20- Ice height by NT1400 (~V)
21-28- Ice temperature 1-8, roughly 1, 2, 3, 4, 5, 6, 7, 10 m depth at installation (°C)

29- Station tilt in X-direction = east-west direction at installation (~V)
30- Station tilt in Y-direction = north-south direction at installation (~V)
31- GPS time
32- Latitude (ddmm.mmmmm)
33- Longitude (ddmm.mmmmm)
34- Elevation (m)
35- Geoidal height (m)
36- Unit
37- GPS quality
38- Number of GPS satellites
39- Horizontal dilution of precision
40- Temperature in logger enclosure (°C)
41- Current drawn by ventilator in Rotronics assembly (mA)
42- Voltage of batteries before measurements (V)
43- Voltage of batteries after measurements (V)

<u>Transmitted data</u>
1- Date and time (UTC)
2- Air pressure (hPa) - *average*
3- Air temperature by PT100 (°C) - *average*
4- Air temperature by HygroClip (°C) - *average*
5- Relative humidity (~% with respect to water, not ice) - *average*
6- Wind speed (m/s) - *average*
7- Wind direction (° relative to north at installation) - *average*
8- Wind direction standard deviation - *average*
9- Incoming shortwave radiation (~V) - *average*
10- Outgoing shortwave radiation (~V) - *average*
11- Incoming longwave radiation (~V) - *average*
12- Outgoing longwave radiation (~V) - *average*
13- CNR1 casing temperature (°C) - *average*

14- Snow height by SR50 on AWS (~m) - *instantaneous*
15- Surface height by SR50 on stakes (~m) - *instantaneous*
16- Ice height by NT1400 (~V) - *instantaneous*
17-24- Ice temperature 1-8, roughly 1, 2, 3, 4, 5, 6, 7, 10 m depth at installation (°C) - *in-stantaneous*
25- Station tilt in X-direction, east-west direction at installation (~V) - *instantaneous*
26- Station tilt in Y-direction, north-south direction at installation (~V) - *instantaneous*
27- GPS time- *instantaneous*
28- Latitude (ddmm.mmmmm) - *instantaneous*
29- Longitude (ddmm.mmmmm) - *instantaneous*
30- Elevation (m) - *instantaneous*
31- Horizontal dilution of precision - *instantaneous*
32- Current drawn by ventilator in Rotronics assembly (mA) - *instantaneous*
33- Voltage of batteries (V) - *instantaneous*

34- Air pressure (hPa) - *instantaneous*

35- Air temperature by PT100 (°C) - *instantaneous*
36- Relative humidity (~% with respect to water, not ice) - *instantaneous*
37- Wind speed (m/s) - *instantaneous*
38- Wind direction (° relative to north at installation) - *instantaneous*
39- Wind direction standard deviation - *instantaneous*

Calculation of physical quantities

All raw measured variables are outputted in useable physical units, with the exception of the following.

Shortwave and longwave radiation
The PROMICE logger program multiplies all four radiation readings (shortwave in&out (SR), longwave in&out (LR); output in mV) by a factor 100 to better resemble flux values (W/m^2). In the processing stage the output is recalculated into μV units, and divided by the calibration coefficient C (in $\mu V/(W/m^2)$) as provided by the sensor's manufacturer. Incoming and outgoing longwave radiation also needs an adjustment for sensor casing temperature. Recalculation:

$SR = SR * 10 / C_{SR}$
$LR = LR * 10 / C_{LR} + 5.6704e^{-8} (T_{CNR1})^4$

where sensor casing temperature T_{CNR1} is in Kelvin ($=T_{CNR1}(°C)+273.15$).

Ice height
The pressure transducer is drilled into the ice a few meters to a few tens of meters, enclosed in a closed system of a liquid that is non-freezable at common Greenlandic temperatures (pure antifreeze or an antifreeze & water mixture). As surface ice melts, the station will lower with it, and the pressure of the vertical liquid column on the pressure transducer will decrease. Wintertime accumulation cannot be recorded by pressure transducer. A wintertime increase in pressure transducer output indicates a higher pressure on the hose lying on the surface caused by a snow pack. This signal cannot be translated in accumulated mass and should be disregarded.
In processing the data, the voltage output is recalculated into a vertical liquid column over the sensor. This id done by multiplying the output value by a constant coefficient (C_{pt}) as determined from a four-point calibration performed by the manufacturer, and adjust for density of the liquid:
$H_{pt} = H_{pt} * C_{pt} * \rho_w / \rho_m$
where ρ_w is the density of water at room temperature (998 kg/m^3) and ρ_m is the density of the liquid/mixture in the pressure transducer system at the approximate ice temperature (see Table 4):

- 100% ethylene glycol = ~1150 kg/m^3 around 0 °C
- 50/50 ethylene glycol & water mixture = ~1090 kg/m^3 around 0 °C

For more accurate determination, GEUS calibrations and exact values for ρ_m as determined at GEUS can be found in the AWS metadata.

Specific Gravity from www.engineeringtoolbox.com							
Temperature	Ethylene Glycol Solution (% by volume)						
(°C)	25	30	40	50	60	65	100
-40	frozen	frozen	frozen	frozen	1.12	1.13	frozen
-17.8	frozen	frozen	1.08	1.10	1.11	1.12	1.16
4.4	1.048	1.057	1.07	1.088	1.1	1.11	1.145
26.7	1.04	1.048	1.06	1.077	1.09	1.095	1.13
48.9	1.03	1.038	1.05	1.064	1.077	1.082	1.115

Table 4. *Density of the liquid/mixture used for the pressure transduser at approximate temperatures.*

Tilt

Tilt readings in V are multiplied by a factor 10 in the logger to better resemble tilt values in degrees. In the recalculation we remove this factor (Tilt=Tilt/10) and use the following polynomial to obtain tilt in degrees in both 'X' and 'Y' direction:

$\mathrm{Tilt}(°) = [\text{sign of Tilt}] * (-0.49\ \mathrm{abs(Tilt)}^4 + 3.6\ \mathrm{abs(Tilt)}^3 - 10.4\ \mathrm{abs(Tilt)}^2 + 21.1\ \mathrm{abs(Tilt)})$

Note that we strive to place the tilt sensor so that its output resembles mast and radiation sensor tilt within 0.5°, but differences up to a few degrees may occur - chiefly in the X direction (east-west) due to the method of attaching the sensor to the boom.

Corrections

Air temperature by HygroClip

Due to an error by our supplier some of the HygroClips deployed in Greenland measure in a different voltage range than others. For this reason *some* HygroClips have an offset of 40 °C. Correction: T = T – 40.

You may notice that the temperatures as measured by PT100 and HygroClip can differ more than one degree, which cannot be explained by sensor inaccuracies as stated in the manuals. We recommend you use the more accurate PT100 readings.

Relative humidity

Relative humidity is measured with respect to water, i.e. it needs correction at sub-freezing temperatures.

Recalculation:

$RH = RH * e_w / e_i$ for $T < 0$ °C.

Saturation vapour pressure over water e_w (Goff & Gratch):

$$\log_{10} e_w = -7.90298\,(373.16/T-1) + 5.02808\,\log_{10}(373.16/T)$$

$$- 1.3816\ 10^{-7}\ (10^{11.344\ (1-T/373.16)}\ -1) + 8.1328\ 10^{-3}\ (10^{-3.49149\ (373.16/T-1)}\ -1) + \log_{10}(1013.246)$$

Saturation vapour over ice e_i (Goff & Gratch):

$$\log_{10} e_i = -9.09718\ (273.16/T - 1) - 3.56654 \log_{10}(273.16/T) + 0.876793\ (1 - T/273.16) + \log_{10}(6.1071)$$

with T in Kelvin (= T(°C)+273.15) and e_w and e_i in hPa. We use PT100 temperatures for calculation.

After this the values may need a small offset correction based on calibration of the sensor upon return from the field.

Wind direction
When metadata indicate that the wind sensor / AWS is not north-south aligned, a (possibly time-dependent) offset value is added / subtracted. Correction: WD = WD +/- offset. We are working on a solution with a compass to keep track of station orientation.

Shortwave radiation
Shortwave radiation measurements are highly sensitive to the tilt of the radiation sensor, which is the main reason why PROMICE AWSs are equipped with a tilt sensor. Since the incoming shortwave radiation correction is complicated and relies on a number of assumptions, we leave the correction of the data to the user. For assistance in performing this correction, or to obtain IDL code to do it for you, data users can contact Dirk van As (GEUS).

Snow and surface height by sonic ranger
Sonic ranger observations are sensitive to air temperature since the speed of sound depends on the density of the medium that it travels through. The distance H as measured by both sonic rangers is corrected as follows:

H = H * (T/273.15)^0.5

with T in Kelvin (= T(°C)+273.15). We use PT100 temperatures for calculation.

Ice temperatures
Note: As with all observations, the vertical position relative to the surface of the measured ice temperatures changes depending of the time of year, though most sensors have a fixed height after the wintertime accumulation has melted away. Keep in mind that, depending on the net mass balance at the AWS site, the thermistor string will melt out in two or more years.

Data overview
Since the start of PROMICE in 2007 we have collected a large amount of data from the AWSs on the ice sheet. We have collected 43% of all available data records in the field up to September 2009, and of the remaining periods received 22% as transmitted data since the last station visits. Data gaps have occurred (11%) due to malfunctioning data loggers

(all of these older data logger types have been replaced by a new type since). In other instances (9%) data quality has been reduced by a station either being blown over by extreme winds, or having fallen into a crevasse. The remainder of the coverage (14%) is from stations that have ceased their transmissions since the last station visit, which is related to a threshold we built into the station's logger program: if battery power drops below a certain value the station will continue to operate, but without power-consuming functions such as transmissions. At our next station visits we will collect the available data. Table 5 gives the overview of the data coverage from the PROMICE automatic weather station. Added together, we have a 65-79% coverage of useable data up to now. The problems with the power supply (yellow color in the chart) will be solved next summer, while all data loggers of the type used in 2007 – some of which were malfunctioning (grey) – have already been replaced by a more reliable logger type. Problems related to crevassed terrain and wind damage (red) will be a recurring theme for automatic weather stations in the ablation zone of the Greenland ice sheet. As we gather more experience with these stations and regions they are placed in, we should be able to reduce the occurrence of similar problems in the future.

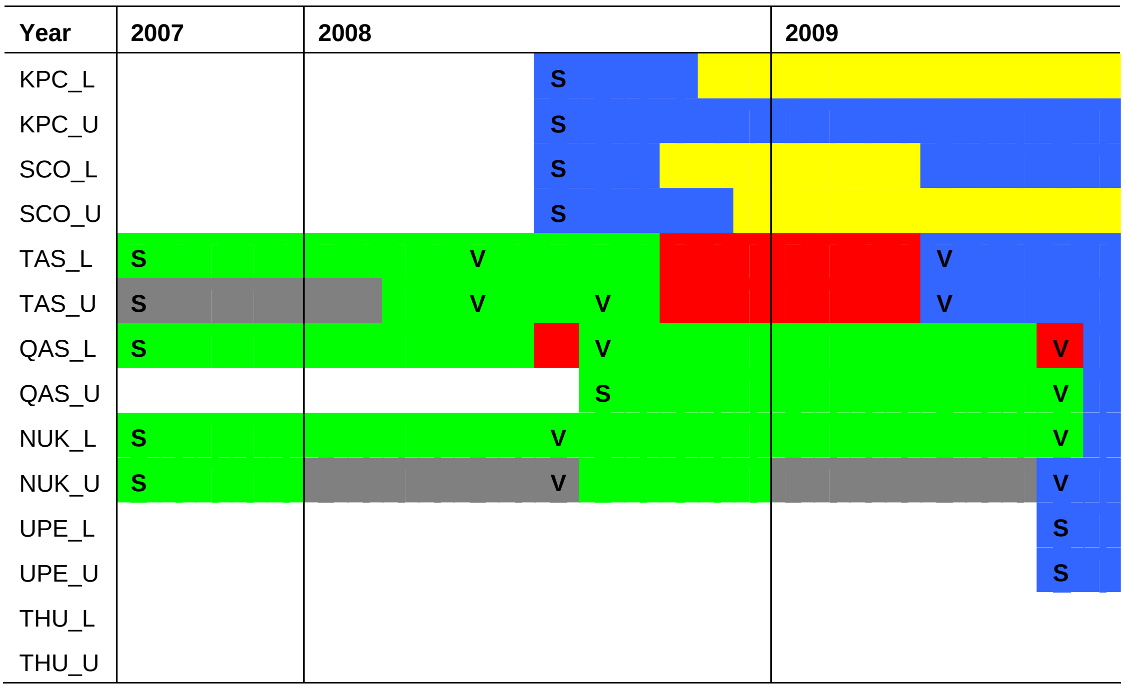

Table 5 *Data coverage chart since the start (S) of each PROMICE automatic weather station. Green indicates that data have been collected in the field. Blue: transmitted data received. Yellow: no transmitted data; data has to be collected in the field. Red: data record complete, but station blown over or in a crevasse. Grey: data gap due to logger malfunction. V: station visit.*

Development of a new calving model for numerical ice flow modelling

Calving of icebergs accounts for perhaps as much as half the ice transferred from the Greenland Ice Sheet into the surrounding ocean, and virtually all of the ice loss from the Antarctic Ice Sheet. Recent observations have shown that changes in calving rate can greatly reduce the extent of floating ice shelves and ice tongues, potentially resulting in increased discharge from the interior [Joughin et al, 2004; Rignot et al., 2004]. While the break-up of floating ice tongues has no direct effect on global sea level, the resulting speed up of grounded ice can have dire consequences for global sea level. Indeed, a wide range of observations applying to both current ice masses and paleo ice sheets, point to iceberg calving as a major factor in rapid ice-sheet changes [Van derVeen, 2002]. It is, therefore, important to formulate a calving model that can be readily incorporated into time-evolving numerical ice-flow models.

We have formulated a calving model that can be readily incorporated into time-evolving numerical ice-flow models. This new calving criterion is based on a physical model of calving processes.

Our model is based on downward penetration of water-filled surface crevasses and upward propagation of basal crevasses. A calving event occurs when the depth of the surface crevasse (which increases as melting progresses through the summer) reaches the height of the basal crevasse.

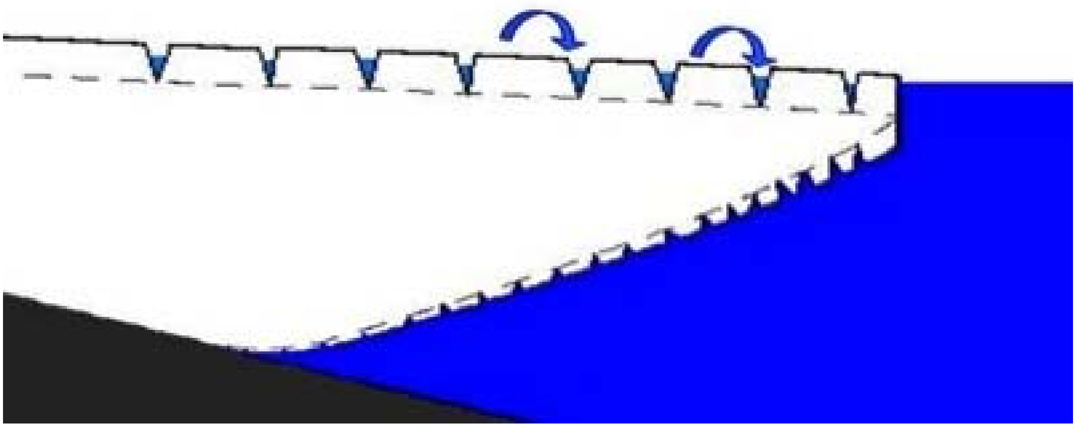

Figure 20. *Diagram showing the calving mechanism*

Ice flow model

The calving model has been implemented into a numerical ice flow model that calculates the flow and evolution of the geometry, which is based on the model used in *Nick et al.* [2009].

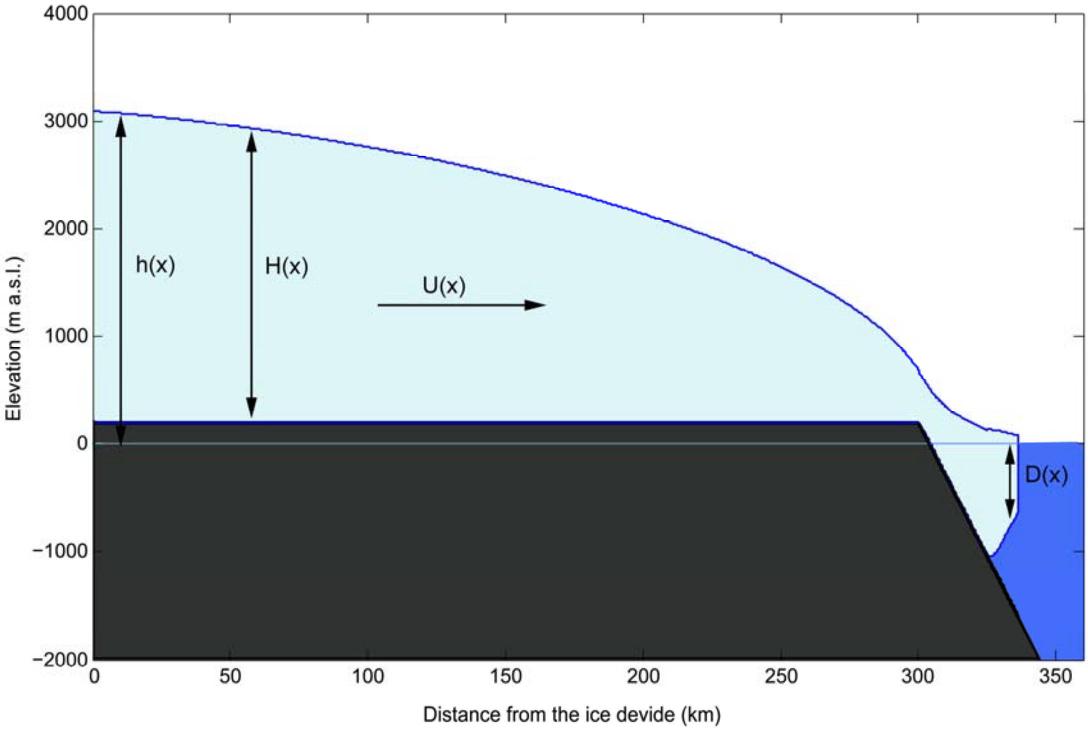

Figure 21. *Geometry of the model*

Continuity and force balance

Considering a flowband of width W and thickness H, conservation of mass is expressed by the depth-integrated continuity equation [Van derVeen, 1999; Oerlemans, 2001]. Vertically-integrated model includes (Longitudinal, lateral, basal stresses)

$$\frac{\partial H}{\partial t} = -\frac{1}{W}\frac{\partial q}{\partial x} + a \qquad (1)$$

where t is time, x is the distance along the central flowline, a is the surface mass balance. Neglecting the effect of sloping sidewalls, the horizontal ice flux through a cross section of the flowband is given by q=HWU, with U the vertically-averaged horizontal ice velocity.

Conservation of momentum requires [Vieli and Payne, 2005]

$$2\frac{\partial}{\partial x}\left[H\nu\frac{\partial U}{\partial x}\right] - \mu A_s\left(\left(H - \frac{\rho_i}{\rho_p}D\right)U\right)^{\frac{1}{n}} - \frac{2HB}{W}\left(\frac{5U}{W}\right)^{\frac{1}{n}} = \rho_i g H\frac{\partial h}{\partial x} \qquad (2)$$

A_s and μ are the sliding and friction parameter. *v* is the strain-rate dependent effective viscosity.

Boundary Conditions

The upglacier boundary (x = 0) corresponds to the ice divide where the surface slope and horizontal velocity are set to zero. At the calving front, the longitudinal stress is balanced by the difference between hydrostatic pressure of the ice and water, giving for the stretching rate at the terminus

$$\frac{\partial U}{\partial x} = \left[\frac{\rho_i g}{4B} \left(H - \frac{\rho_p}{\rho_i} \left(\frac{D^2}{H} \right) - \frac{\sigma_B}{\rho_i g} \right) \right]^n \qquad (3)$$

σ_B is the back pressure from sea ice or sikkusak. ρ_P is the density of sea or lake water.

The second boundary condition at the terminus is the calving criterion. Using the new calving model, the glacier terminus calves off when the sum of the basal and surface crevasse depths reaches the glacier thickness. This calving criterion allows formation of an ice shelf or a floating tongue when this sum is smaller than the flotation thickness. The transition between grounded ice and shelf is achieved through setting basal resistance to zero; that is, the friction parameter, μ, in Equation (10) is set to zero when the ice thickness becomes less than the flotation thickness.

Results

Our numerical ice sheet model is able to reproduce observed seasonal changes of Greenland outlet glaciers, such as fluctuations in flow speed and terminus positions. We have applied the model to Helheim Glacier on the east coast. The model is capable of reproducing the recent rapid changes of Helheim Glacier (See Figure 22).

Our model suggests that rapid retreat of the calving front is highly affected by the amplified calving rate due to increasing water level in surface crevasses during warmer summers. Our results show little response to seasonally enhanced basal lubrication from surface melt.

This modeling study provides insights into the role of surface and basal hydrology to ice sheet dynamics and on how to incorporate calving in ice sheet models and therefore advances our ability to predict future ice sheet change. Perhaps the most important finding here is that the physically-based calving model directly linked to climate, reproduces seasonal retreat and advance of the glacier terminus.

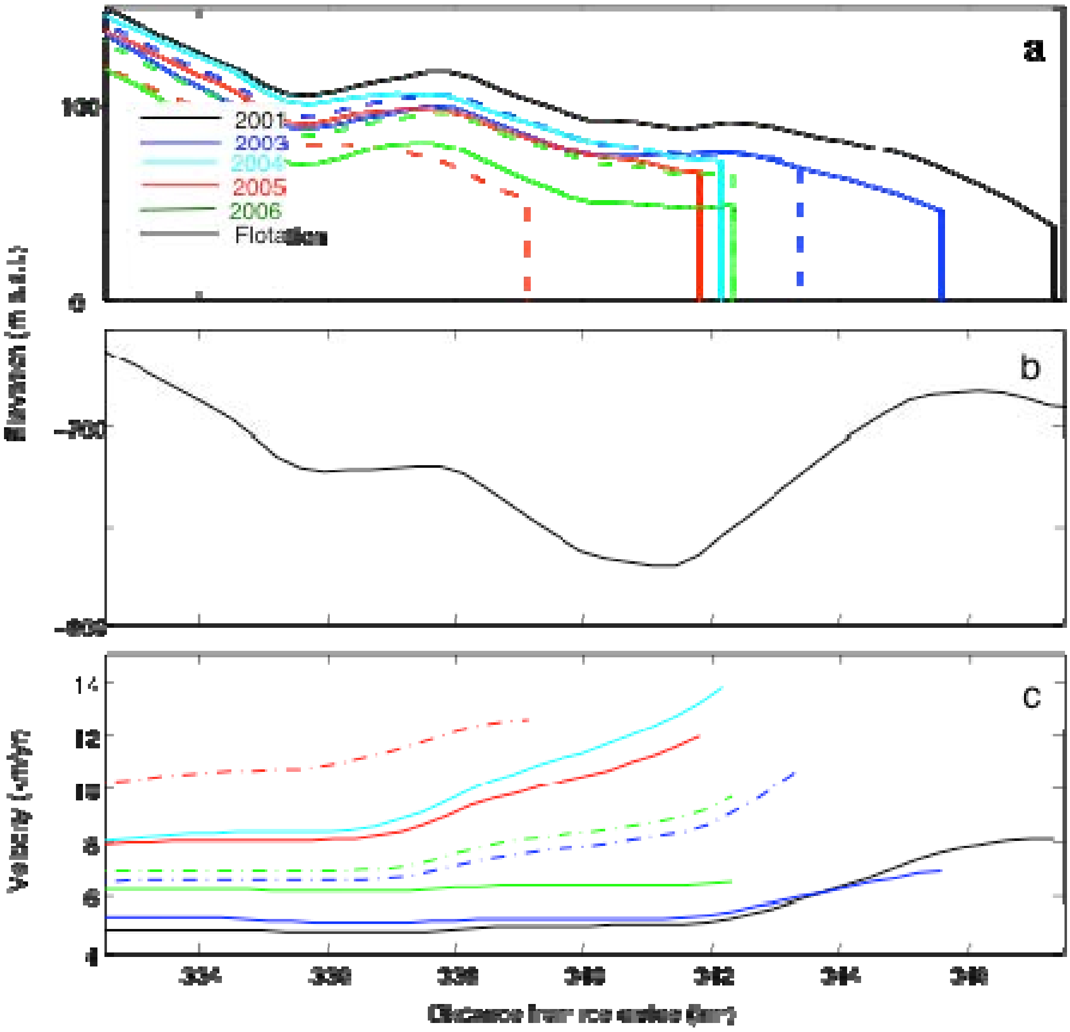

Figure 22. *Surface (a) and velocity profiles (c) along the flow line near the ice front in the water level experiment. The solid lines correspond to the beginning of the summer season, while the dashed-dotted lines correspond to the end of summer for different years. The dotted line in (a) shows the flotation height, above which the glacier is grounded. (b) The glacier bed topography based on the data from the University of Kansas.*

In conclusion, while there are refinements that can be made to better quantify climate forcing on outlet glaciers, our model experiments are robust as to outlet glacier response to these external forcings.

References

Joughin, I., W. Abdalati, and M. Fahnestock (2004), Large fluctuations in speed on Greenland's JakobshavnIsbræ glacier. *Nature 432*, 608-610.

Nick, F.M., A. Vieli, I.M. Howat, and I. Joughin (2009), Large-scale changes in Greenland outlet glacier dynamics triggered at the terminus. Nature Geoscience, doi: 10.1038/NGEO394.

Oerlemans, J. (2001) Glacier and climate change. A.A. Balkema, Amsterdam.

Rignot, E., D. Braaten, S.P. Gogineni, W.B. Krabill, and J.R. McConnell (2004), Rapid ice discharge from southeast Greenland glaciers. *Geophysical Research Letters 31*, L10401, doi:10.1029/2004GL019474.

Van derVeen, C.J. (1999), Fundamentals of Glacier Dynamics. Rotterdam: A.A. Balkema, 462 pp.

Vieli A. and A. J. Payne (2005), Assessing the ability of numerical ice sheet models to simulate grounding line migration, Journal of Geophysical Research 110, 1-18.

Publications

Nick, F.M., A. Vieli, I.M. Howat, and I. Joughin (2009), Large-scale changes in Greenland outlet glacier dynamics triggered at the terminus. Nature Geoscience, doi: 10.1038/NGEO394.

F.M. Nick, C.J. Van derVeen, A. Vieli, D. Benn (2009). A physically based calving model applied to investigate recent changes of Greenland outlet glaciers. (In preperation)

Conference contribution

2008 AGU Fall Meeting, F.M. Nick, C.J. van derVeen, A. Vieli, D. Benn; A calving law for ice sheet models; Investigating the role of surface melt on dynamics of Greenland outlet-glaciers.

Mapping of glacier and ice sheet extent

In the first year (2007), contacts within Denmark and abroad have been established and preliminary work on defining the workflow for glacier mapping from optical remote sensing data has been carried out. Five key activities have been defined:

1. Build and maintain an up to date knowledge of new data resources becoming available over time and of the operative status of satellite platforms such as Terra/ASTER, which have already reached their planned service life.
2. Define a suitable standard workflow for producing ice margins maps and change assessments based on existing remote sensing datasets
3. Improve the cooperation between PROMICE and leading international research groups and projects active within GLIMS (Global Land Ice Measurements from Space) by cooperating in producing some initial batches of geospatial information to be contributed to the GLIMS database
4. Establish the relevant expertise to move from the use of available remote sensing imagery to the scheduling of new satellite observations, including obtaining the required authorizations
5. Publish the relevant results in peer reviewed journals and through scientific meetings

Glacier monitoring from optical remote sensing is being carried out within the GLIMS (Global land Ice Measurement from Space) framework, where GEUS serves as the regional Center for Greenland. During early 2007 Dr. Frank Paul (University of Zurich – Irchel, Switzerland) visited geus as a guest researcher to enable knowledge transfer on the methodological aspects, and some preliminary spatial datasets were produced, analyzed, and reported during the XXIV IUGG General Assembly in Perugia (Italy).

Science output

Some 2007 preliminary results for Disko Island (See Figure 23) are shown in the following figures detailing the size distribution of glaciers in 2001 and the glacier length change from the end of the Little Ice Age (LIA) to 2001 (See Figure 24)

One oral presentation to an international meeting has been delivered:

- Ahlstrøm, A.P., Paul, F., Jepsen, H., Citterio, M., Solgaard, A.M. & Andersen, S.B. 2007: Glacier retreat on Disko Island, West Greenland. IUGG 2007 Perugia, XXIV IUGG General Assembly. 2-13 July, 2007. Perugia, Italy. International Union of Geodesy and Geophysics

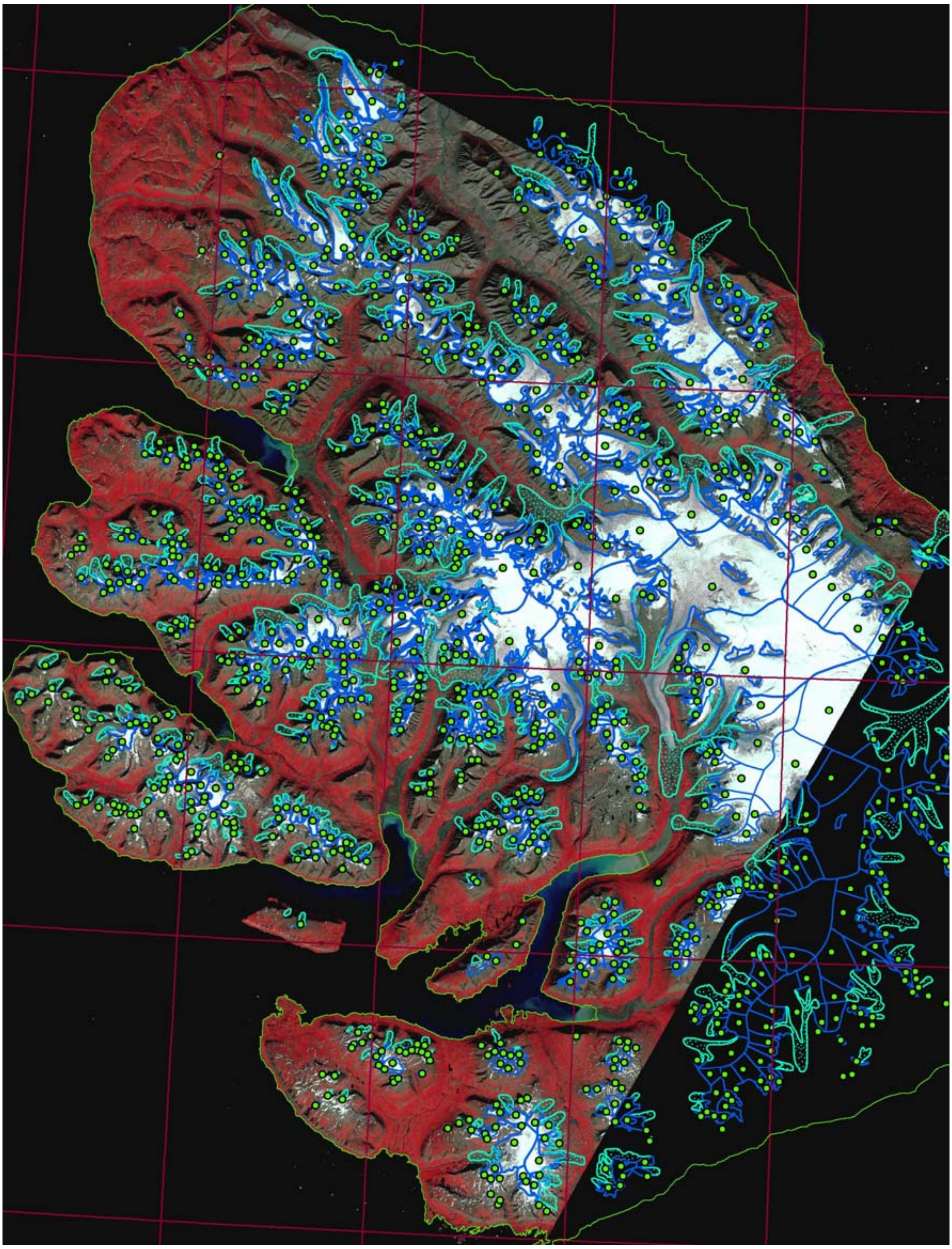

Figure 23. *False colour Landsat ETM+ scene of Disko Island from 2001, and vectorized glacier outlines from the West Greenland Glacier Inventory (WGGI) showing the Little Ice Age (LIA) extent in light blue and the inventory outline in blue. Green dots mark inventory metadata locations.*

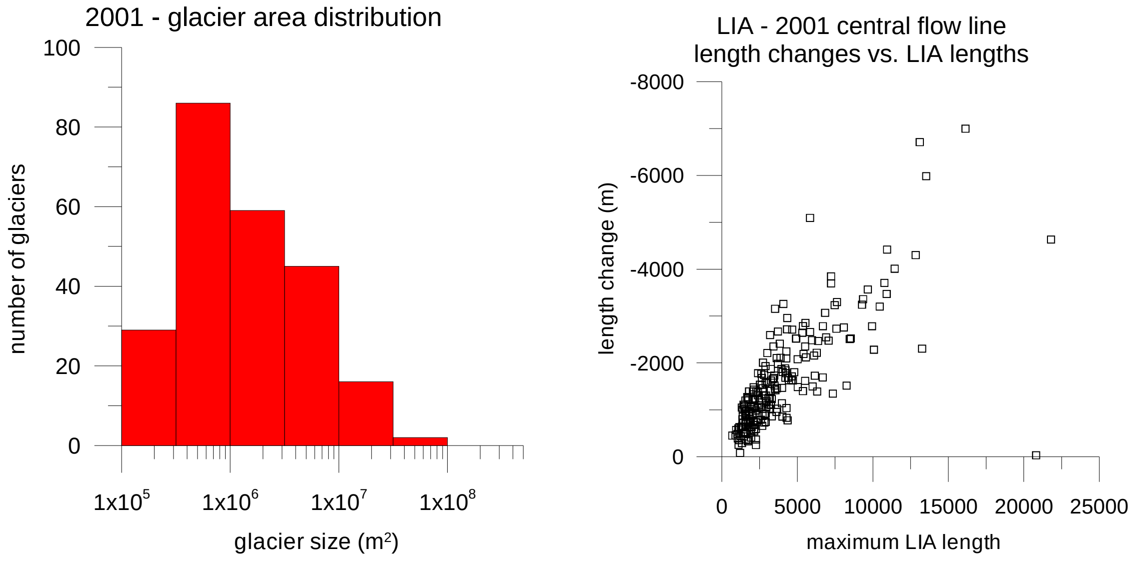

Figure 24. *Left: Size distribution of Disco Island glaciers in 2001. Right: Length change of Disko island glaciers from LIA to 2001*

Completion of the workflow for glacier mapping

During 2008 the workflow for glacier mapping from optical remote sensing data has been completed, and an exercise on a test area in West Greenland has been carried out. The five key activities defined during 2007 and discussed above §1.14 have been implemented on an operative basis.

With reference to point 1 above (build and maintain an up to date knowledge of new data resources becoming available over time and of the operative status of satellite platforms such as Terra/ASTER, which have already reached their planned service life), a very significant development was the gradual release for access at no cost of archived Landsat data by USGS. The free availability of this high quality dataset made possible to easily experiment with many different scenes from the same areas during the definition of the processing workflow, much in the same way as it was already possible with ASTER data through the involvement in the GLIMS project.
As to the operational status of the Terra/ASTER sensor, data in the SWIR bands from late April 2008 to the present exhibit anomalous saturation of values and anomalous striping. This problem is attributed by NASA/JPL to an increase in ASTER SWIR detector temperature believed to be caused by increased thermal resistance in the SWIR cryocooler. VNIR and TIR bands are unaffected by this problem, and continue to show excellent quality, meeting all mission requirements and specifications. It must be noted that the SWIR bands are of no particular interest to glaciological applications, and their failure therefore doesn't impact PROMICE use of the Terra/ASTER data.
The ASTER Global Digital Elevation Model (GDEM) is a new interesting product which has been announced to become available during early 2009. *(update: ASTER GDEM has been released to the public on 29 June 2009 and the available coverage for Greenland has been downloaded and archived at GEUS).*

Finally, information has also been acquired on the sensors specifications and data availability for ESA products.

With reference to points 2 (define a suitable standard workflow for producing ice margins maps and change assessments based on existing remote sensing datasets) and 3 (improve the cooperation between GEUS and leading international research groups and projects active within GLIMS by cooperating in producing some initial batches of geospatial information to be contributed to the GLIMS database) listed above, a test area in West Greenland between 69 and 72 °N covering Disko Island, Nuussuaq Peninsula and Svartenhuk Peninsula was selected to evaluate the most suitable methods and define the workflow to map ice margins and assess their fluctuations from optical remote sensing datasets. The data processing and interpretation work was started in cooperation with Frank Paul (University of Zurich – Irchel, Switzerland) and covered all phases required to produce a vector glacier outline map from the raw satellite imagery, in particular:

- selecting suitable satellite imagery
- raster image processing to enhance the multispectral image and filter noise
- raster processing for multispectral land classification based on a thresholded band ratio method
- topologically controlled raster to vector conversion
- manual editing to address specific issues such as debris covered ice
- manual interpretation of surface geomorphology to map the Little Ice Age position of the ice margins
- geospatial processing to produce a glacier change assessment
- geospatial analysis to produce spatial averages and trends of the quantified parameters
- producing statistics of glacier extent and glacier change

A more detailed overview of these results is summarized below.

With reference to point 3 above (improve the cooperation between PROMICE and leading international research groups and projects active within GLIMS by cooperating in producing some initial batches of geospatial information to be contributed to the GLIMS database), GEUS is now part of the GlobGlacier Users Group. GlobGlacier is a major international project funded by the European Space Agency and led by Frank Paul (University of Zurich – Irchel, Switzerland) aimed at filling the most significant gaps in the GLIMS database by mapping glacier outlines in several regions of the world. PROMICE involvement covers the validation phase of the glacier mapping products based on the aerial photographs, topographic maps, and other information available from GEUS archives and databases. Annual meetings in Zurich are being attended on a regular basis.

With reference to point 4 above, the relevant expertise has been acquired through contacts with Bruce Raup (University of Colorado at Boulder/NSIDC) and Leon Maldonado (NASA/JPL). This covers the custom programming of such instrument settings for the in-orbit ASTER sensor as the hardware amplifier gains for the individual channels of the visual and infrared bands. Properly specifying of these non-standard hardware settings is fundamental during the submission of a new acquisition request for PROMICE use. This is due to the typical high albedo of the target areas, which combined with the sun elevation in polar areas calls for a specific calculation based on the latitude and day of the year. Authorization for direct access to the observation scheduling system of the Terra/ASTER mission has been applied for (ASTER DAR Tool). (*update: the DAR Tool authorization has been granted during 2009 and the first images where acquired during summer 2009*).

With reference to point 5 above (Establish the relevant expertise to move from the use of available remote sensing imagery to the scheduling of new satellite observations, including obtaining the required authorizations), a manuscript has been submitted to the Annals of Glaciology, and two more contributions to international scientific meetings have been produced*. (update: the manuscript has been accepted and is now in press in Annals of Glaciology vol. 53)*.

These works reported on various aspects and on the results of glacier mapping and change assessment in the Disko Island, Nuussuaq Peninsula and Svartenhuk Peninsula. Apart from demonstrating the suitability of the adopted methods for operational use, the manuscript contributes an original approach to estimating the accuracy of a glacier change assessment from optical remote sensing over an area hosting a large number of surge-type glaciers. This approach is based on finding well constrained upper and lower bounds to the glacier change estimate, and is summarized in more detail below.

First results from the glacier mapping

The local glaciers and ice caps on Greenland are of particular interest for automated glacier mapping from thresholded band ratios of multispectral satellite data, as they have been only partly mapped, mainly during the 1940s–60s, and their potential contribution to global sea-level rise could be large. Using three Landsat ETM+ scenes from 2001 covering Disko Island (Qeqertarsuaq) and the Nuussuaq and Svartenhuk peninsulas, West Greenland (See Figure 25), the glacier extent in 2001 was mapped for 1172 glaiciers.

Little Ice Age (LIA) extents from clearly visible trimlines were digitized for a subsample of 500 glaciers. In this region with numerous surge-type glaciers, the related area-change calculation is challenging. This was addressed by considering two different samples with and without known surging glaciers. For the three regions the mean area changes are –28%, –20% and –23%, respectively, when known surge-type glaciers are excluded. It is interesting to note that smaller glaciers tend to have undergone a markedly stronger retreat with respect to their original size than the larger ones, with the total number of glacier increasing due to fragmentation of larger fglaciers into smaller ones (See Figure 26 a, b).

The glaciers on smaller islands and peninsulas closer to the margin of the ice sheet showed a lower mean area change of –15%. Moreover, lower (–16%) and upper (–21%) bounds are calculated for the overall area changes in the entire region between the LIA and 2001 using different upscaling assumptions. Cumulative length changes since the LIA were found to be slightly lower for surge-type glaciers. While dependence of the relative area change on glacier size (for specific size classes) is similar to that in other regions, a distinct spatial distribution of glacier change has been observed. In general, glaciers closer to the sea showed larger changes compatible with a more maritime climate (See Figure 27). A formal assessment of the accuracy of the mapped glacier outlines is difficult since all outlines have been visually controlled and corrected against the Landsat image.

The overall accuracy of the glacier change estimate, including uncertainties related to unclear geomorphological evidences in outlining LIA extents and the related upscaling to the entire sample, has been constrained as by deriving upper and lower bounds for the change. In this context, it is worth summarizing how these bounds derive from two contrasting assumptions: (1) that all glaciers without a recognizable LIA trimline in the terminus forefield have remained stable (or even advanced), and (2) that the subsample of glaciers with recognizable LIA extents is representative of the whole sample. The first assumption leads to underestimation of the glacier change (it sets a lower bound), since it is clear that the LIA trimline could have been obliterated or simply made too uncertain to interpret. As to the second assumption, any stationary or advancing glacier would invalidate it, since we would not have been able to recognize and digitize any LIA outline for such a glacier, thus excluding it from the analyzed subsample and overestimating the change.

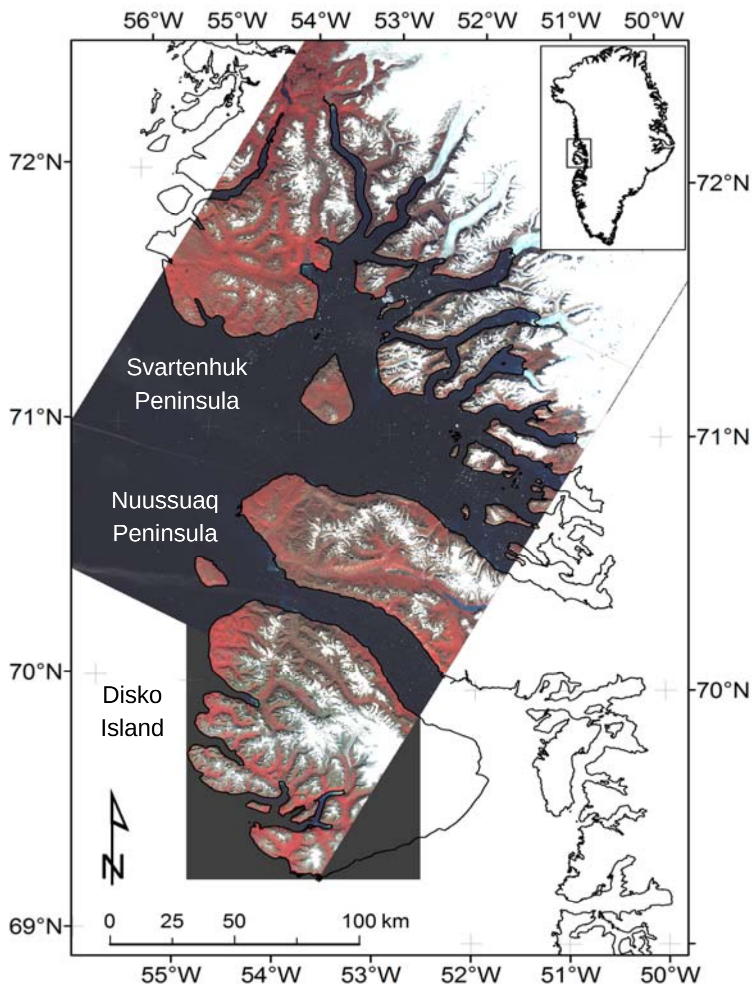

Figure 25. *Overview showing the location of Disko Island, Nuussuaq Peninsula and Svartenhuk Halvo (West Greenland) basd on the three Landsat ETM+ scenes from August 8th, 2001 used in this study. In the inset, the outline of Greenland and the location of the study site are indicated.*

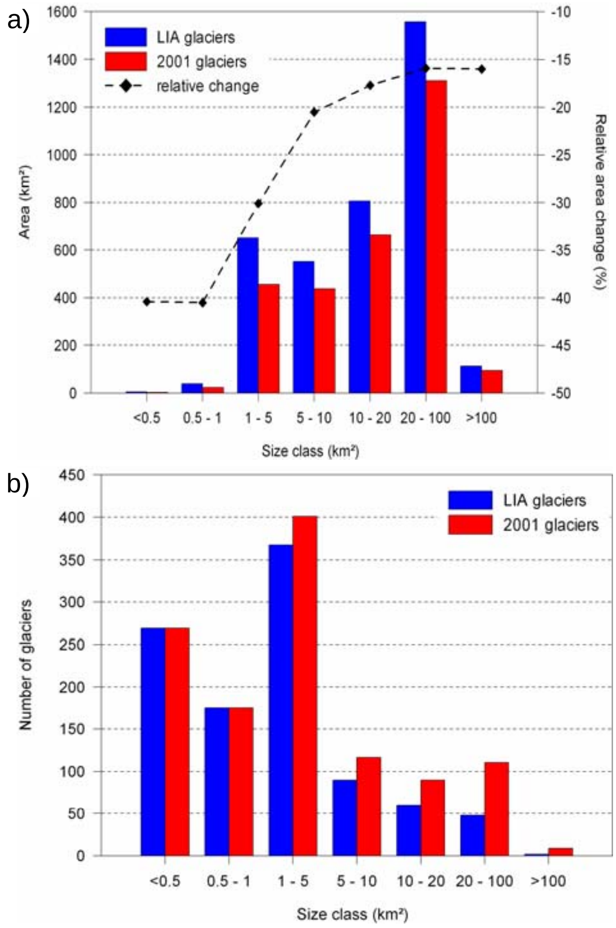

Figure 26. *a) Comparison of glacierized area covered in every given size class, together with the relative area change, only considering glaciers for which the LIA extent is available; b) number of glaciers in the entire sample in the LIA (blue) and 2001 (red).*

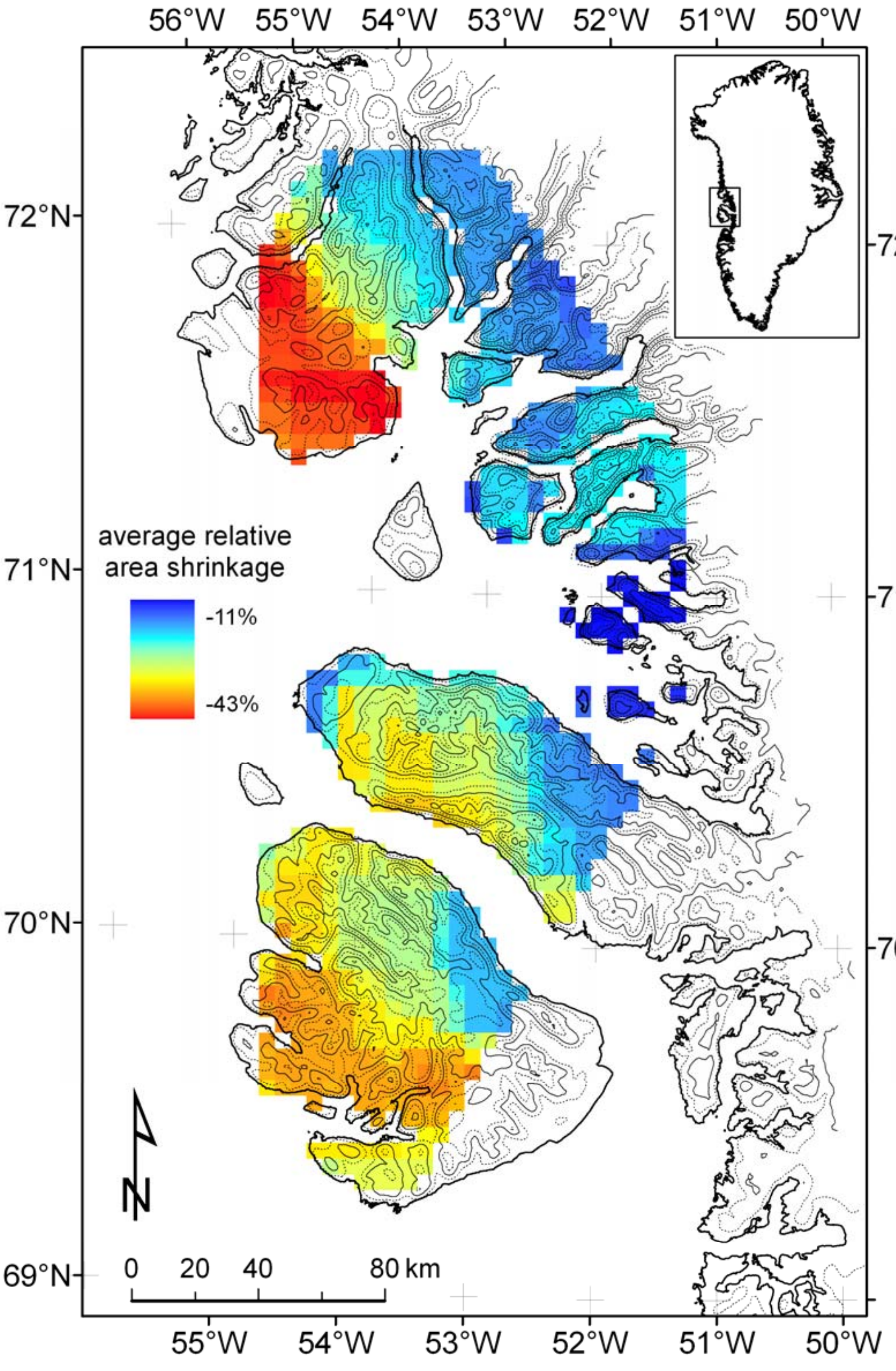

Figure 27. *Spatial variability of the LIA to 2001 relative area change over the entire region computed as 50 km x 50 km average of glacier change. Yellow to red colours mark areas with larger change, blue areas smaller changes.*

One manuscript has been submitted to an internation peer reviewed journal:

- Citterio M., Paul F., Ahlstrøm A.P., Jepsen H.F. & Weidick A. (in press): Remote sensing of glacier change in West Greenland: accounting for the occurrence of surge-type glaciers. Annals of Glaciology vol. 53

Two oral presentations to international meetings have been delivered:

- Citterio, M., Paul, F., Ahlstrom, A.P., Jepsen, H.F. & Weidick, A. 2008: Remote sensing of glacier change on Disko Island, Nuussuaq Peninsula and Svartenhuk Halvø (West Greenland) since the Little Ice Age. 33rd International Geological Congress 2008. 6-14 August, 2008. Oslo, Norway. International Geological Congress Committee (IGCC). Abstract volume

- Paul, F., Citterio, M., Ahlstrom, A.P., Jepsen, H.F. & Weidick, A. 2008: A new inventory of local glaciers and ice caps for part of West Greenland: methods, challenges and change assessment. International Workshop on World Glacier Inventory. 20-21 September, 2008. Lanzhou, China. International Glaciological Society. Abstract volume

Airborne survey of ice sheet elevation and thickness with scanning laser altimetry and ice-sounding radar

A Riegl LMS-Q140i-60 near infrared laser scanner and the DTU-developed 60 MHz icesounder was flown on a DeHavilland DHC-6 Twin Otter registered under OY-POF chartered from Air Greenland. The ice-sounder uses radio pulses to measure the distance between aircraft and the ice surface and the distance from the ice surface to the bedrock. From those distances the ice thickness is calculated. When the conditions permit acquisition of laser scanner data of the ice surface, the ice-sounder surface measurements are replaced by the laser measurements having much higher accuracy. The aircraft position was recorded by three onboard geodetic GPS receivers sampling at 1 Hz corresponding to a flight distance of approximately 70 m. The three GPS receivers were connected, via splitters, to either the front or the rear aircraft GPS antenna. The sampling frequency of the laser-scanner was 40 scan lines each with 250 measurements per second while the ice-sounder recorded 3.125 samples/second (after pre-processing).

The ice-sounder worked continuously during the complete flight mission, but was not active during the transits between the airport and the ice edge. To optimise the bedrock detection with the radar a low flight altitude is preferred, i.e. about 1,000 ft, and down to 100 ft in some areas. The radar was not able to detect the bottom in some areas near the ice edge mainly due to heavily crevassed ice and in some areas in the southern part of Greenland probably due to water in the ice. Figure 28 shows the flight track and where a bottom echo was obtained.

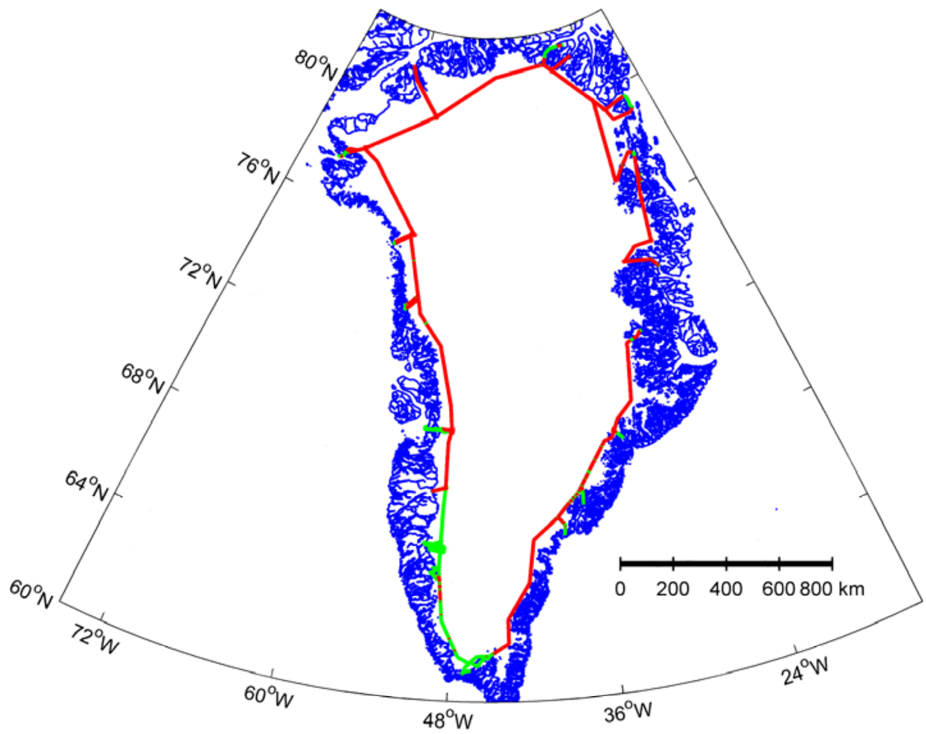

Figure 28. *The flight path with transits excluded. Green segments show where a bottom echo was detected, while red segments show where a bottom echo was not detected.*

GPS data

The GPS position data was processed by using a PPP (Precise Point Positioning) software developed partly at Wuhan University and partly at National Space Institute, DTU Space, providing latitude, longitude and height above the WGS84 ellipsoid of the GPS antennas. The solutions were compared with differential GPS solutions from Trimble GPSurvey 2.35 to evaluate the robustness of the positions. Both PPP and GPSurvey rely on precise GPS products from IGS (International GNSS Service).

Data from the different GPS receivers was compared and quality controlled, and the best solution selected for further use. The GPS data were transferred to the laser scanner and ice-sounder instruments by adding the positions of these instruments inside the aircraft relative to the GPS antenna positions to the GPS data.

Lidar data

Surface elevation data was derived from laser altimeter measurements made concurrently with the radar measurements and using the same INS and GPS set up to derive positioning information. The Riegl scanning laser used to make the elevation measurements, provides cross-track scans with a range accuracy better than 5 cm. Absolute elevations are given with a precision of ±0.3 m following processing. The laser operates in the near-infrared wavelength band and has a scan angle of 60°, giving a swath width similar to the flight elevation above the ground. Over the glacier surface, a typical value of this distance was 300 m. Roll, pitch, heading, and yaw of the aircraft were recorded at 50 Hz by a Honeywell

H764-G, medium-grade INS (Inertial Navigation System). The orientation and the position of the aircraft with respect to the earth fixed reference system are used to exactly map each laser measurement to a position on the surface.

Data acquisition and processing - Ice-sheet bottom echo

The ice-sounder data acquisition consists of transmitting pulses at a pulse repetition frequency of 5kHz (i.e. the sampling in the flight direction) and sampling the returned echo at 75MHz in range producing 4096 samples per transmitted pulse. While internal scattering masks the desired echo, reflection and absorbsion within the ice-sheet reduces the strength of the returned echo. Substantial processing is therefore required to produce a radargramme that makes detection of the ice-sheet bottom echo possible. This radargramme processing is done both on-line during acquisition and off-line using software developed at the Microwave & Remote Sensing division, DTU-Space. An example of a radargramme obtained by the icesounder is displayed in Figure 29, where the horizontal direction represents the time with a spacing of 320 ms per line (i.e. 22.4 m spacing at aircraft velocity 70 m/s). The vertical direction shows propagation time of the radar pulse with a spacing of 80 ns per line of the radar pulse. This represents vertical distances but not by simple scaling because the speed of light within the ice-sheet is lower than in free air. The transmit pulse is also visible in the radargramme, because echo data sampling is started before the transmit pulse begins. This early starting of data sampling ensures calibration of the propagation delay.

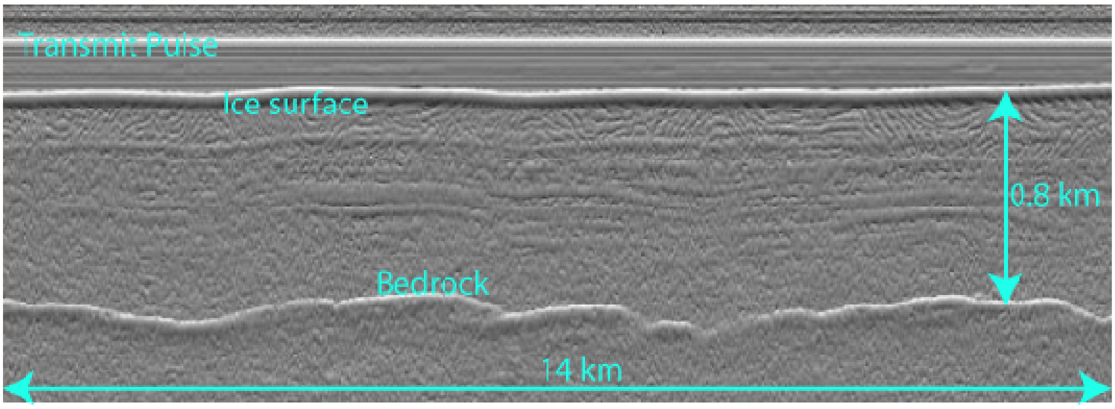

Figure 29. *Radargramme showing transmit pulse, ice surface, and bedrock echo.*

The processing of the ice-sounder data was performed by using a semi-automatic layer (bottom and surface) detection programme developed at the Microwaves & Remote Sensing division, DTU Space. The detection programme detects each layer individually, hence the following detection procedure is performed for both surface and bottom. The detection processes is initiated by the user selecting a pixel in the radargramme that is part of the layer to be detected. This pixel is located in one particular vertical line. The automatic part of the programme then selects the pixel (left or right) within a specified search angle in a neighbouring vertical line that shows the strongest contrast to its neighbouring samples in the same line. This second pixel then becomes the basis for the automatic selection of the third pixel and so forth. There may be multiple echoes from the bedrock at some locations with rough bedrock. In such cases it may be impossible to se which echo is from vertical beneath the aircraft and which echo comes from the bedrock slightly off the flight track.

This algorithm works well in areas with good layer echoes. In other areas the automatic detection looses track of the layer wherefore the user must manually set the pixel for each vertical line in such areas. As the layer (both bottom and surface) may not be detectable everywhere, the outcome of this process is a number of intervals of consecutive verticals lines with a pixel defining the layer. The positions of all these pixels in terms of UTC-time, GPS position, and propagation time are recorded to a file.

Ice surface elevation, ice thickness and bottom elevation
UTC-time or GPS-time is recorded by all of the GPS-position-, laser scanner-, and, icesounder instruments and is used as reference for aligning the three different types of observations. At the time of the mission, the GPS-time is given as UTC-time plus 14 seconds.

The calculation of ice thickness and bedrock elevation requires the surface elevation to be known; hence ice thickness and bedrock elevation is not calculated in areas where the ice surface could not be measured with neither the scanner nor the radar.

The ice surface elevation can be measured with either the scanner or with the radar, but the two sensors does not detect the same surface. The scanner detects the optical surface usually perceived as the surface while the radar pulse is reflected approximately 12 m below the optical surface. This difference has been measured by comparing measurement over the Kangerlussuaq runway with measurements over the ice. As the scanning laser altimeter is far more accurate than the radar, scanner data has been used for calculating the surface elevation where available. However, due to fog or malfunction scanner data was not available everywhere and radar data was then used instead. As the 12 m difference only applies over ice and as all radar data recordings including parts without ice were requested, no surface elevation correction was applied in areas where radar data was used. In stead the radar data product contains information as to which sensor was used for each calculation of the surface elevation. However, this surface difference was corrected for in the calculation of ice thickness and bottom elevation as shown below.

Replacing scanner data with radar data for ice surface detection poses a special problem when flying close to the ice surface. Oscillations from the radar transmit pulse masks the received echo from the ice surface when the distance from the radar to the ice surface is below approximately 200 m. A new processing technique has reduced this distance to 120 – 150 m. However, when radar data has been used to detect the ice surface and this distance is detected to be below 150 m the ice surface altitude must be considered less reliable and in theory this distance could be anywhere between 0 and 120 m. This uncertainty translates into an uncertainty for the bottom elevation of 52 m.

The ice surface elevation (given as height above the ellipsoid) of a point along the flight track is calculated by subtracting the aircraft to surface distance d_{surf} measured by the laser scanner from the GPS-measured aircraft ellipsoidal height. The horizontal position of the surface point is given by the horizontal GPS coordinates.

The ice thickness of a point along the flight track is given by

$d_{ice} = 84.5\ (T_{bot}-T_{sur})+12$

where d_{ice} is the thickness of the ice in meters. T_{bot} is the propagation time (echo delay) in microseconds of the radar signal bottom echo and T_{sur} is the propagation time in microseconds of the radar signal surface echo. T_{bot} is measured by the radar.

When laser data are available T_{sur} is calculated by

$T_{sur} = T_{pulse} + (d_{surf}+d_{cable}+12)/150$

where T_{pulse} is the propation time in microseconds of the radar transmit pulse, d_{surf} is the distance in meters from scanner to ice surface and d_{cable} is the equivalent free air length of the radar to antenna cable.

When laser data are not available T_{sur} is taken from the radar measurements and is calculated as

$d_{surf} = 150(T_{sur} - T_{pulse}) - d_{cable}-12$

in order to provide the surface elevation. The bottom elevation is obtained by subtracting the ice thickness from the surface elevation. All elevations are in WGS84 ellipsoid coordinates.

Starting up method development of satellite-derived surface-velocity calculation

The objective of the 2008 activities at DTU within PROMICE are was preparation of a software processing chain capable of measuring the three-component ice velocity from Synthetic Aperture Radar (SAR) data.

The following techniques are well established for the task and were therefore selected for the project:

- SAR Interferometry (InSAR)
- Image correlation techniques, known in literature as speckle-, coherence- and feature-tracking methods. These will be jointly referred to as offset-tracking techniques in the following.

The activities were decomposed into Work Packages (WPs), as shown in 29.

WP		PROMICE at DTU in 2008/2009: updated Jan. 12th 2009																				Days
WP		Description Year		2008						2009												Days
		Year Month	6	7	8	9	10	11	12	1	2	3	4	5	6	7	8	9	10	11	12	
		Project Month	1	2	3	4	5	6	7	8	9	10	11	12	13	14	15	16	17	18	19	
1		**Preparation of standard InSAR processing chain**				56																
	1.1	Order machine and install OS + GAMMA modules	3																			3
	1.3	Focusing script update & test runs (archive data)	3																			3
	1.4	Interferogram formation script preparation & test runs	10	10																		20
	1.5	Geophysical inversion module script preparation & test runs		10		20																30
		WP sub total																				**56**
2		**Performance of standard proc. chain on develop. data set**									54											
	2.1	Development data set definition (archive data)					3															3
	2.2	InSAR processing of development data set					3															3
	2.3	Analysis and consolidation of standard InSAR chain					15															15
	2.4	Offset tracking script preparation & test runs						15														15
	2.5	Offset tracking processing of development data set								3												3
	2.6	Analysis and consolidation of standard offset tracking chain								10	5											15
		WP sub total																				**54**
3		**Developments of the standard proc. chain**										20										
	3.1	Error prediction for InSAR (interface to existing DTU software)										5										5
	3.2	Error prediction for offset tracking										5										5
	3.3	Fusion Module design										5										5
	3.4	Vector velocity derivation - implementation and testing										5										5
		WP sub total																				**20**
4		**Validation**													60							
	4.1	CAT-1 project (application for ESA-distrbuted data access)								3												3
	4.2	Validation data set definition (areas of interest, tracks and frames)									5											5
	4.3	Fusion module implementation and testing											15									15
	4.4	Processing of validation data set											5									5
	4.5	Data analysis												12								12
	4.6	Processing chain corrections												5	10							15
	4.7	Documentation of procedure													5							5
		WP sub total																				**60**
5		**Operational processing of 100 x 400 km area**																23				**23**
6		**Delivery to GEUS**																	19			**19**
7		**Operational processing of 3 areas, each 100 x 400 km**																			69	**69**
		Meetings	KO							M1					M2				M3			**278**

Figure 30. *Schedule for PROMICE activities at DTU in 2008/2009*

In order to ensure updates to future sensors and algorithms and assistance in using the software, a commercial software package distributed by the Swiss consortium GAMMA Remote Sensing and Consulting AG, was selected to provide the core processing modules. This package is referred to as the “GAMMA software” in the following and in 29.

The work carried out in year 2008 covers WP-1 through WP-2.4, corresponding to a total of 92 effective working days. It includes development and testing of the SAR image focusing and InSAR processing chains as well as a preliminary implementation and testing of the offset-tracking chain. Testing during this phase is carried out on a data set in DTU’s archives, referred to as the “development data set”.

The 2009 activities will comprise 186 effective working days. The first step is a consolidation of the offset-tracking processing chain, which concludes WP-2. The output of WP-2 is a “standard processing chain”, capable of producing map-projected InSAR slant-range displacement and topography measurements as well as offset tracking slant-range and azimuth displacement ones, using data acquired from a single satellite track. The “azimuth” dimension coincides with the satellite flight direction, whereas the “slant-range” dimension is orthogonal to the azimuth one and oriented along a straight line from the SAR to a point on ground.

WP-3 and WP-4 provide additional necessary functionalities for the project, to be developed at DTU, namely measurement error standard deviation estimation for topography and

slant-range and azimuth displacements, conversion of the displacement measurements to radar-independent coordinates and fusion of multiple-track height and displacement measurements. Testing in this phase is to be carried out on the development data set but also on a newly ordered validation data set, comprising images from the most recent SAR sensor data distributed by the European Space Agency (ESA).
The outcome of WP-4 is a validated processing chain, which will be delivered to GEUS and be used at DTU and GEUS for operational processing.

Status

By the end of 2008 WP-1 had been completed and WP-2 had started. This report describes the work carried out in WP-1 and WP-2. This includes work carried out on WP 2 in early 2009 on the offset tracking processing and analysis.

Processing Chain Overview

Functional Blocks

The architecture of the InSAR/offset-tracking software under development is shown in Figure 31.

In a typical processing sequence, the focusing module (FOC) is used to concatenate a certain number of consecutive raw data frames acquired from a single satellite track, and to perform range and azimuth focusing, generating a Single Look Complex product (SLC). Both InSAR and offset tracking techniques require pairs of SLC products to be generated, corresponding to approximately the same ground track.

Each SLC pair is then processed by the offset-tracking module (OTR), which models the registration offsets between non-moving areas in pairs of SLC products with low order polynomials in each image dimension, and accordingly re-samples each pair to a common master SLC geometry. In all cases, SLC or SLC intensity data patches are correlated on a coarse grid (e.g. 3 km) to refine the re-sampling information derived from the orbit state vectors. Optionally, correlations are subsequently also performed on a fine grid (e.g. 100 m), yielding residual registration offsets in the slant-range and azimuth dimensions. Coarse and fine grid registration offsets form an Offset Tracking Product (OTP).

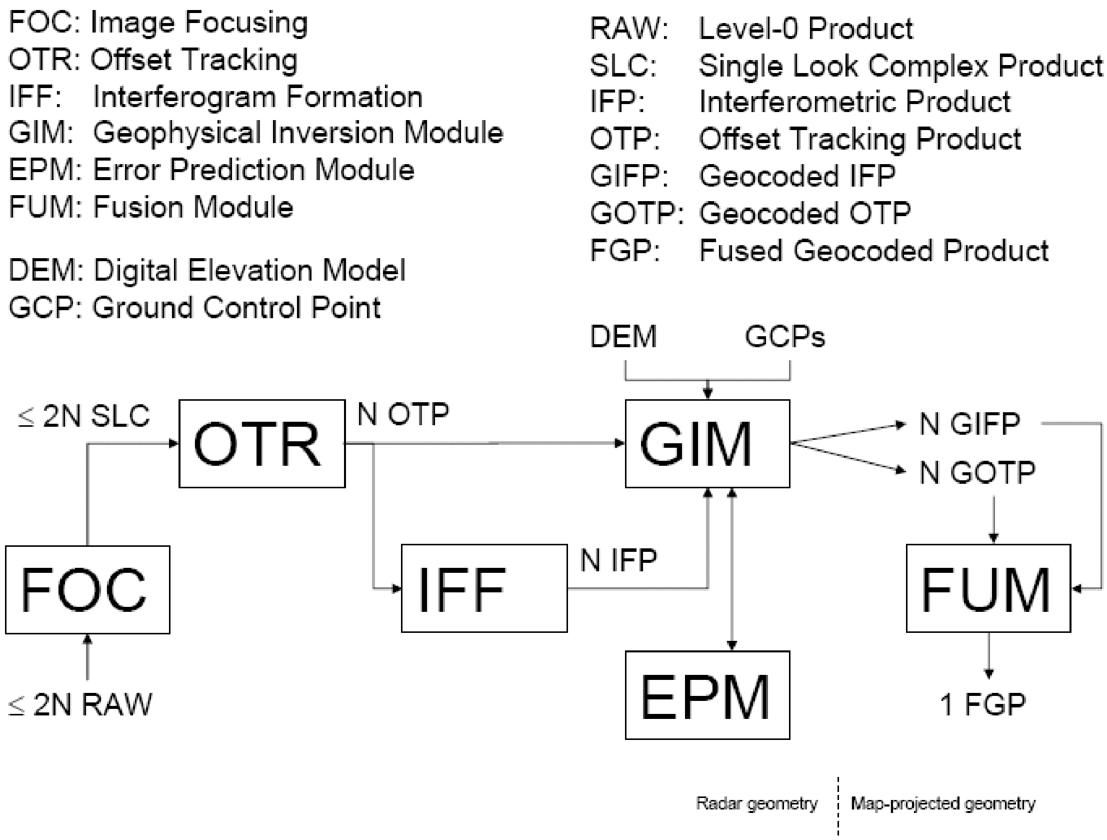

Figure 31. *Processing chain block diagram*

For each SLC pair, if registration offsets were computed only on a coarse grid, the re-sampled SLCs may be input to the Interferogram Formation module (IFF), which will generate an interferometric product (IFP). If SLC registration offsets were computed also on a fine grid, these may be either supplied to the IFF, which will use them to refine the image-registration based on the coarse offsets only, or directly supplied to the Geophysical Inversion module (GIM).

The GIM uses one or more OTP and/or IFP to output map-projected geophysical measurements (displacement and height) and their predicted error measurement standard deviation, generated by the Error Prediction Module (EPM). These form the GIFP (Geophysical Interferometric Product) and the GOTP (Geophysical Offset Tracking) products respectively. The GOTP includes displacement measurements in azimuth and slant-range, whereas the GIFP may contain height and/or slant-range displacement measurements. In general also auxiliary data, namely an external Digital Elevation Model (DEM) and a set of Ground Control Points (GCPs) (points of known height and velocity) will be needed by the GIM to obtain accurate results.
In the FUM, displacement products from single tracks are converted to a coordinate system independent of radar geometry (e.g. east, north, up) and height and displacement measurements from different (and possibly overlapping) tracks are combined to form a Fused Geophysical Product (FGP), which is the processing chain final output.

Implementation

The developed software consists of 5 user-operated Linux executables corresponding to the functional blocks previously described, namely FOC, OTR, IFF, GIM and FUM. The

EPM is instead operated internally by the GIM. These executables make use of those included in the GAMMA software packages as well as a suite of ANSI-C programs developed at DTU.

Combination and testing of the GAMMA executables amount to most of the work in WP-1 and WP-2. This is due to the fact that the GAMMA software comes as a set of Linux executables, thought for general InSAR/Offset-tracking applications. The modules of primary interest for this project, namely the MSP (Modular SAR Processor), ISP (Interferometric SAR Processor) and DIFF&GEO (Differential Interferometry and Geocoding) ones include 57, 92 and 56 executables respectively. Therefore a selection of the supported algorithms is required, as well as a determination of appropriate parameter ranges, based on GAMMA documentation, scientific literature and performance on test-cases.

Additional software development is required to provide utility programs needed to combine the GAMMA executables in the desired way, as well as to implement functionalities not included in the commercial package, but essential for PROMICE.

Implementation details and software usage are considered out of the scope of this report, and will be documented in a Software User Manual, as part of WP-4.7.

Development Data Set

The tests described in the following sections were carried out on an ERS-tandem data set described in Figure 32. It is composed of two ERS-1/ERS-2 tandem acquisitions, referred to as T1 and T2 in Figure 32 and in the following. Each acquisition is composed of 3 consecutive raw data frames, acquired on descending track 325 over north-eastern Greenland.

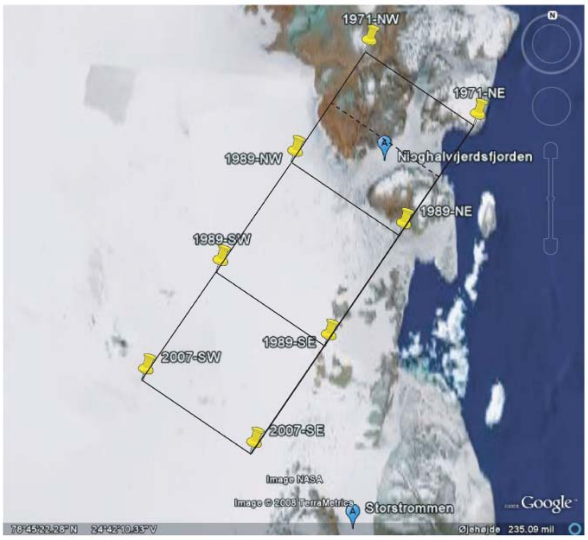

T1, Bperp = -4 m		
Sat	**Orbit/frames**	**Date**
ERS-1	23359/1971-2007	02-Jan-1996
ERS-2	3686/1971-2007	03-Jan-1996

T2, Bperp = 106 m		
Sat	**Orbit/frames**	**Date**
ERS-1	24361/1971-2007	12-Mar-1996
ERS-2	4688/1971-2007	13-Mar-1996

Figure 32. *Development data set coverage. The dashed line indicates the approximate extent of the reference height and displacement data set of Figure 33.*

A height and a 2-D displacement map covering most of this area was kindly provided by Ian Joughin, now at the University of Washington, and used as a reference for the testing of the developed processing chain. It is plotted in a geographic equiangular projection in Figure 33. The average height and slant-range displacement accuracy of the reference data are expected to be 13 m and 3.0 m/y respectively [1].

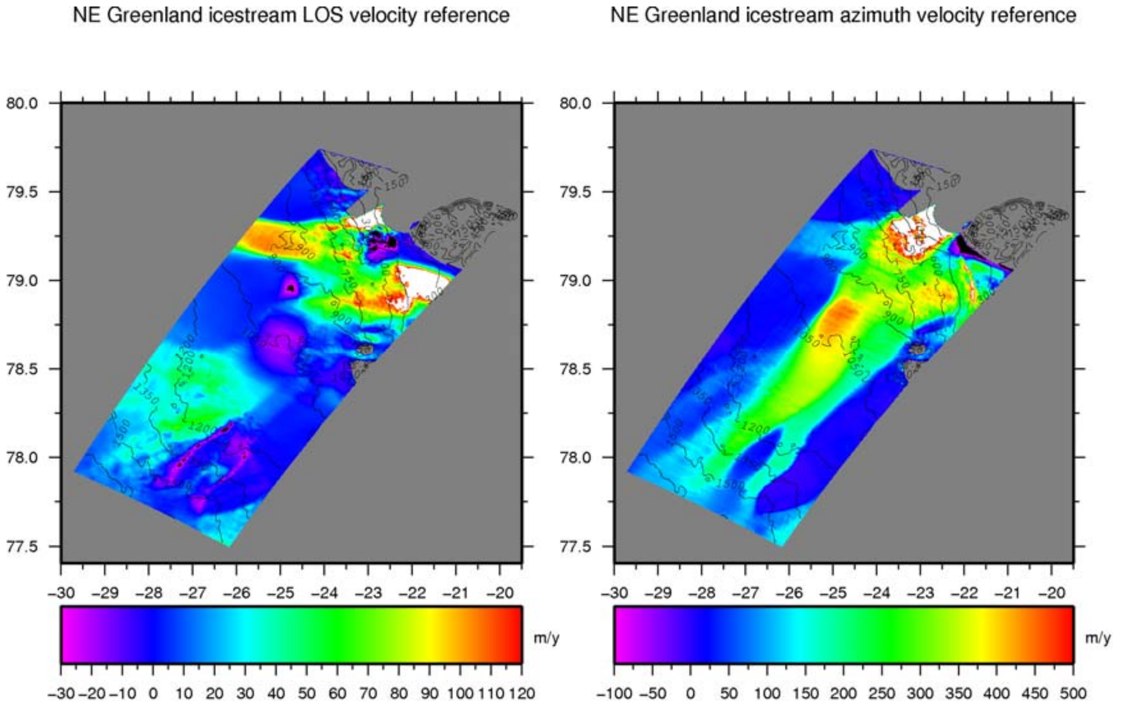

Figure 33. *Line-of-sight (LOS) displacement [m/y] (left) and azimuth displacement [m/y] (right) with superposed WGS-84 ellipsoidal height contour [m]. Data was provided by Ian Joughin, University of Washington, and re-projected from map-geometry to the reference radar geometry of the development data set. LOS measures are positive towards the radar, azimuth ones are positive from bottom to top of the radar image.*

Processing Chain Performance on the Development Data Set

Image Focusing

In order to extract geophysical measurements from the development data set, the FOC was run 4 times, once for each raw data strip composing T1 and T2 (see 31), obtaining 4 SLC products.

A multi-looked intensity image corresponding to ERS-2 orbit 03686 (denoted E2_03686 in the following), is shown in Figure 34 to the left. The image is in radar geometry, averaged by factors 8 x 40 in slant-range and azimuth respectively, corresponding 160 m x 160 m on ground. Due to the descending track acquisition geometry and to the fact that the SAR “looks” to the right, Lambert Land appears to the left of Nioghalvfjerdsfjorden, in the near-range of the radar. A higher radar backscatter is observed, as expected, from areas above the equilibrium located at a height of about 800 m for this region (see the height contours in Figure 33).

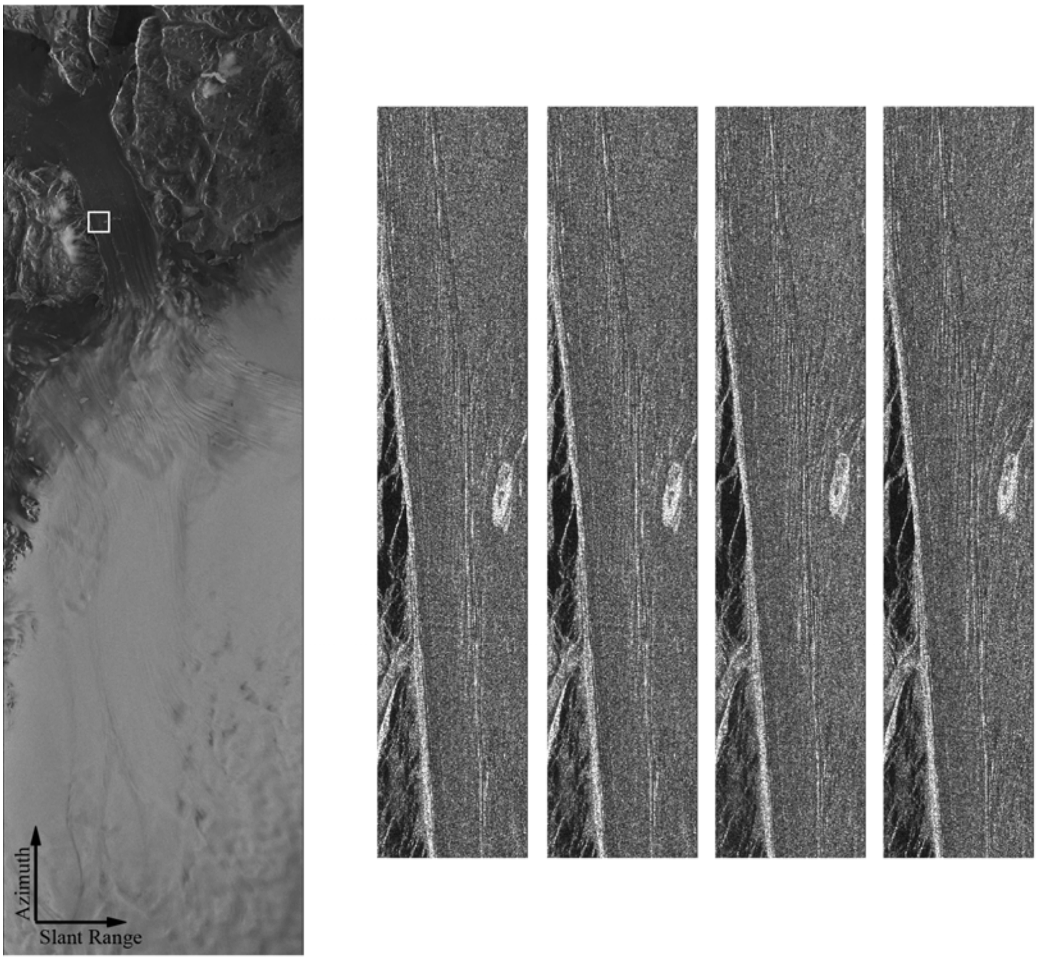

Figure 34. *Left: Multi-looked intensity image of E2_03686 obtained with the FOC module. Right: full resolution resampled SLC magnitude corresponding to area in the white box in the multi-looked image, obtained with the OTR module. From left to right the full-resolution image patches correspond to E2_03686, E1_23359, E1_24361 and E2_04688 respectively.*

Registration offset computation

In a first processing run, the OTR was run on each SLC pair composing T1 and T2, with the objective of registering non-moving areas in each SLC to a common reference geometry, chosen as that of E2_03686.

For each SLC-pair, residual registration offsets compared to orbital information were estimated by computing intensity correlation-peaks on a regular grid (32 x 96 correlations in slant-range and azimuth respectively, corresponding to a 3km x 3km grid on ground). Large correlation windows of size 64 x 256 in slant-range and azimuth respectively were chosen and images were oversampled by a factor 2 prior to correlation. Signal-to-noise-ratio (SNR) was used as a confidence measure for offset estimation. This is defined as the ratio of the correlation peak to the averaged correlation value in a box surrounding the peak. Offsets with an SNR>4.0 were used to estimate 4 polynomial parameters, modelling image misregistration. These were subsequently used to resample each SLC to the reference geometry.

The registered SLC images were visually inspected to verify that point targets in non-moving areas, such as bedrock, had been registered to sub-pixel accuracy. In the case of the T2 SLC pair, the above procedure had to be repeated using an even larger correlation window size of 256 x 1024 pixels, in order to achieve registration with sub-pixel accuracy. Offsets were in this case computed on a coarser grid of 16 x 48 pixels, to improve efficiency.

The magnitude of a small portion of the registered SLC images is shown in Figure 34 (right). The area considered (white box in Figure 34, left) is on the floating glacier tongue of Nioghalvfjerdsfjorden, and includes co-registered static features (bedrock), as well as mis-registered moving ones (e.g. the white disc feature, which might be a frozen meltwater lake).

In a second processing run, the OTR was used on each re-sampled SLC pair, obtained with the procedure described above, to compute residual offsets related to motion. To this end, two different offset-tracking techniques were tested and are described in the following sub-sections.

Intensity tracking

Intensity correlations were computed for the T1 SLC pair using windows 8 x 32 pixels in slant range and azimuth respectively (160 m x 130 m on ground), on a 10 x 50 pixel grid (~200 m on ground). Images were oversampled by a factor two prior to correlation.
Subsequently, range and azimuth offsets were culled using an SNR threshold of 4.0, and a threshold based on the maximum expected offset magnitude. Hole-filling was performed through a weighted interpolation of at least 8 neighbouring points in a radius of 8 offset measurements. Finally a moving average window 7 x 9 in size was used to reduce the variance of the estimates, at the price of a reduced spatial resolution of about 1.2 km x 1.2 km. The results are shown in Figure 36.

Correlation SNRs above threshold are achieved over almost all the image, including featureless ice-sheet areas, with the highest values located in bedrock areas, and the lowest at the margins of rapidly flowing ice (see Figure 33), and where the ice-sheet funnels into the glacier. There is a close relation between SNR and interferometric correlation, Figure 37, indicating that correlation peaks are related to correlated intensities, rather than to visible features.

In the slant-range and azimuth offsets of Figure 36, the regions of fastest ice-flow can be recognised, as compared to the reference measurements, Figure 33. The offsets however require calibration, i.e. removal of a slowly-varying trend, before they can be interpreted as displacement. This step will be carried out within the GIM. In the azimuth offset data, horizontal stripes appear, at a small angle compared to the slant-range direction. These have been observed by several researchers and are known to be due to ionospheric propagation delay [2].

The intensity tracking procedure was repeated for the T2 SLC pair. Due to the low coherence of this data, Figure 38 (left), very low SNRs were achieved and offsets with a very large variance were obtained. The results are not reported, as useful measurements could not be extracted from this data.

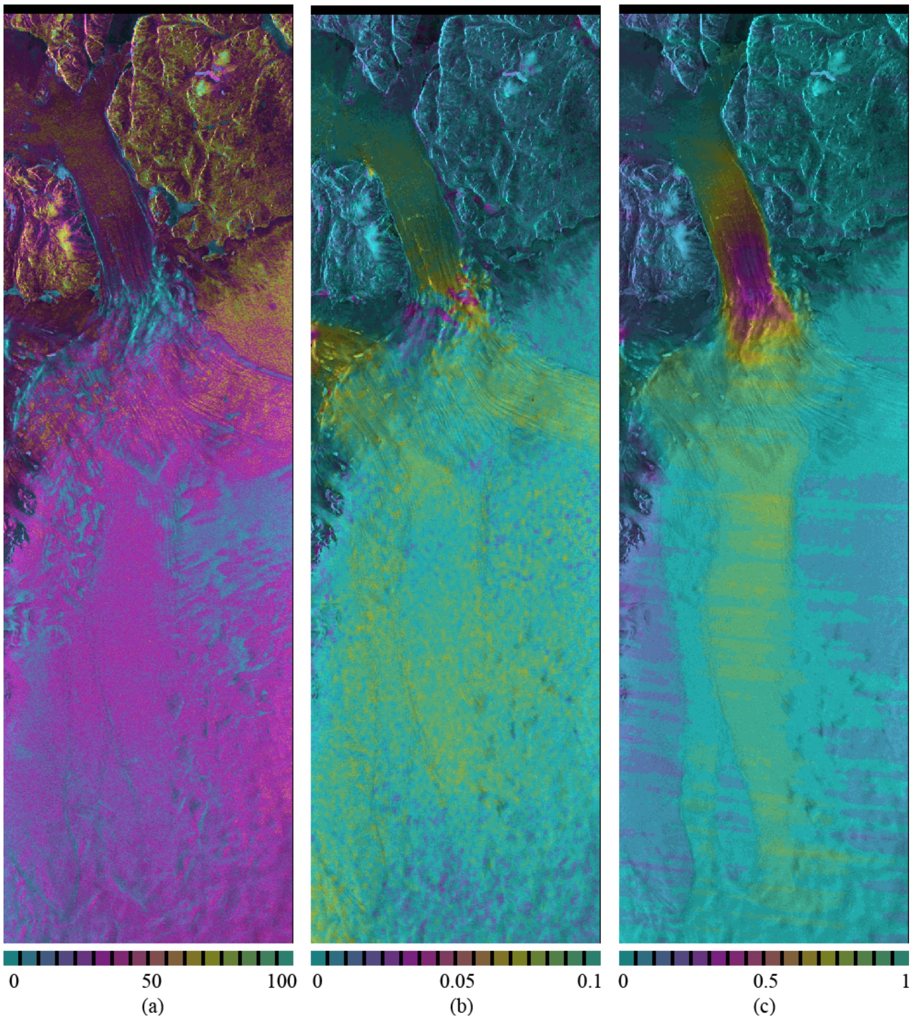

Figure 35. *T1 coherence tracking with an 8x16 correlation window. (a) Offset SNR (b) Slant-range offsets [pixels] (c) Azimuth offsets [pixels]. Slant range and azimuth pixel sizes are respectively 8 m and 4 m. Image brightness is based on a multi-looked intensity image of E2_03686.*

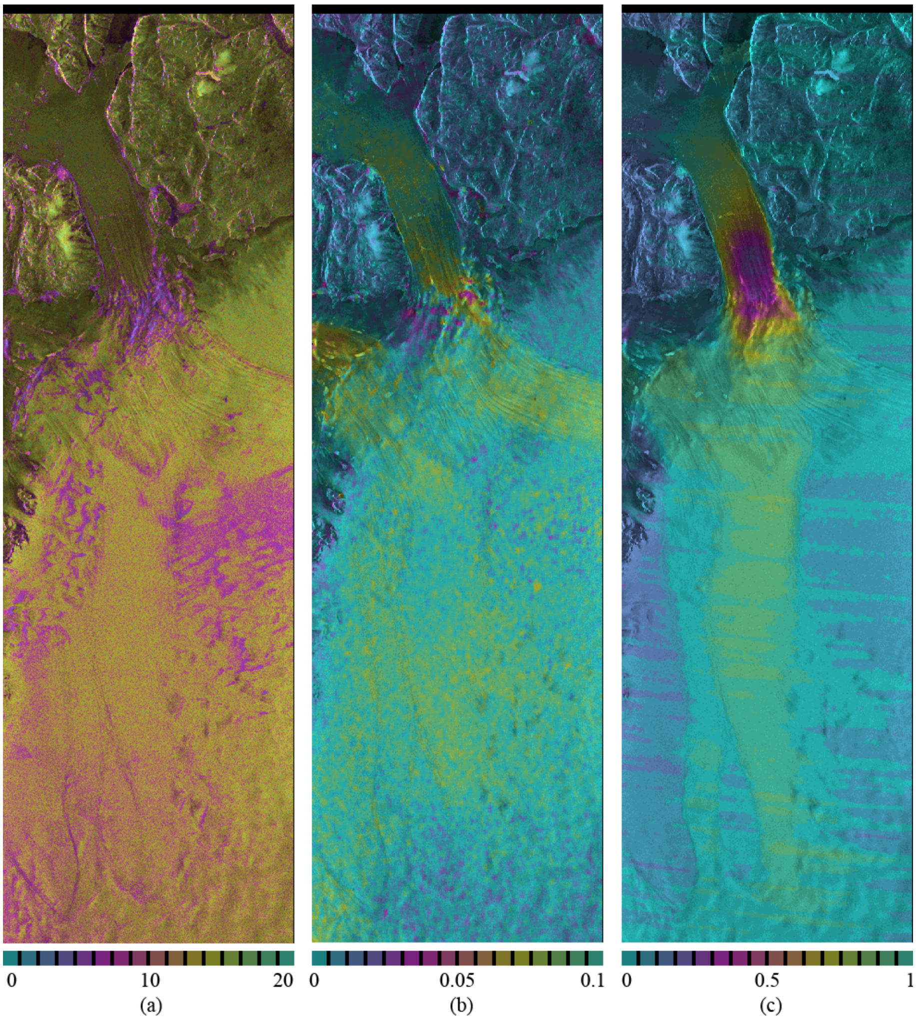

Figure 36. *T1 intensity tracking with an 8x32 correlation window. (a) Offset SNR (b) Slant-range offsets [pixels] (c) Azimuth offsets [pixels]. Slant range and azimuth pixel sizes are respectively 8 m and 4 m. Image brightness is based on a multi-looked intensity image of E2_03686.*

Coherence tracking

Slant-range and azimuth offsets maximising interferometric coherence were computed using windows 8 x 16 in slant range and azimuth respectively (160 m x 65 m on ground), on a 10x50 pixel grid (~200 m on ground). Subsequently, range and azimuth offsets were culled using an SNR threshold of 2.5, and a threshold based on the maximum expected offset magnitude. The same hole-filling and moving-averaging parameters used for intensity tracking were chosen. Results are shown in Figure 35. Although the SNR values are much higher than those in Figure 36a, the spatial pattern is very similar and related to coherence. The spatial pattern of range and azimuth offsets are also similar to those obtained for intensity tracking, Figure 36, including the ionospheric streaks which appear in the azimuth offsets.

Interferogram Generation

The IFF was run on the registered T1 and T2 SLC-pairs output by the OTR, obtaining two interferograms. The IFF performed common-band filtering, phase flattening to the WGS-84 ellipsoid, phase averaging of approximately 22 independent samples (using a 3 x 15 averaging window in slant-range and azimuth respectively) and coherence estimation on approximately 300 independent samples. For T1, the intensity-tracked offsets were used to refine the SLC resampling performed by the OTR, prior to the above mentioned operations. The wrapped interferometric phase and coherence estimates are shown in Figure 37 for T1.

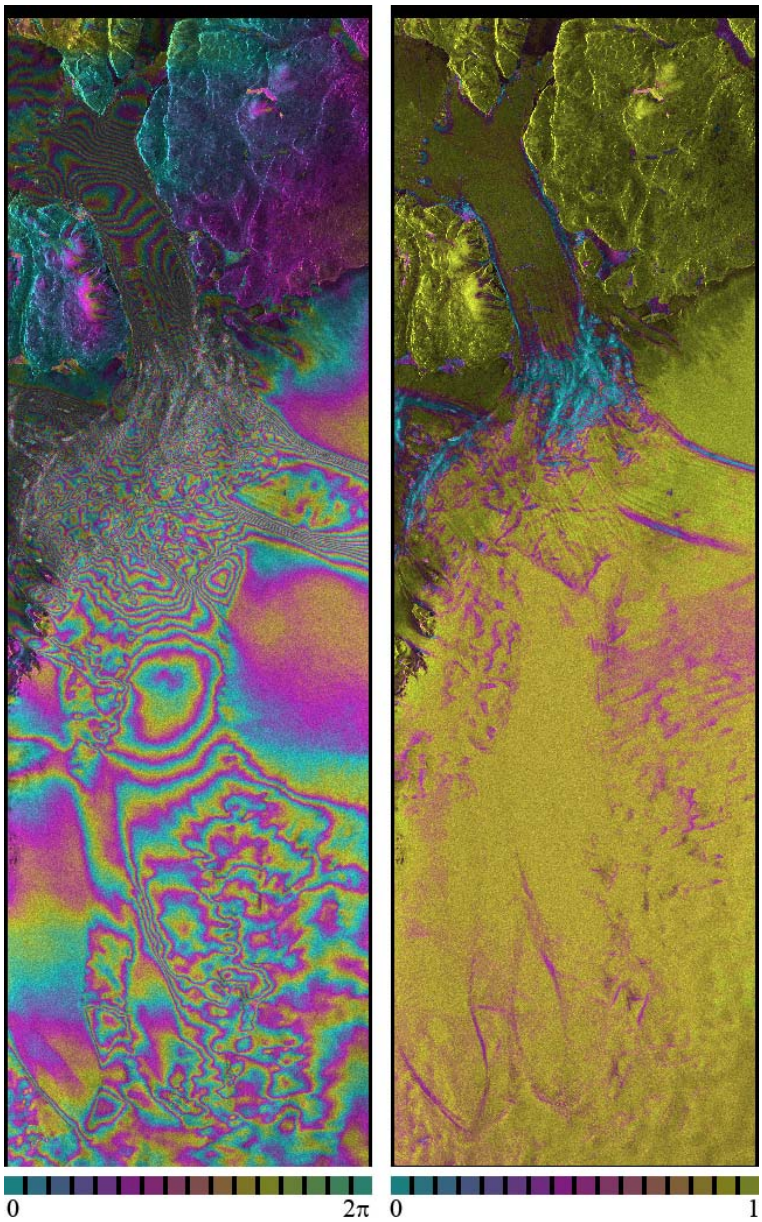

Figure 37. *Interferometric phase (left) and coherence (right) for T1, output by the IFF.*

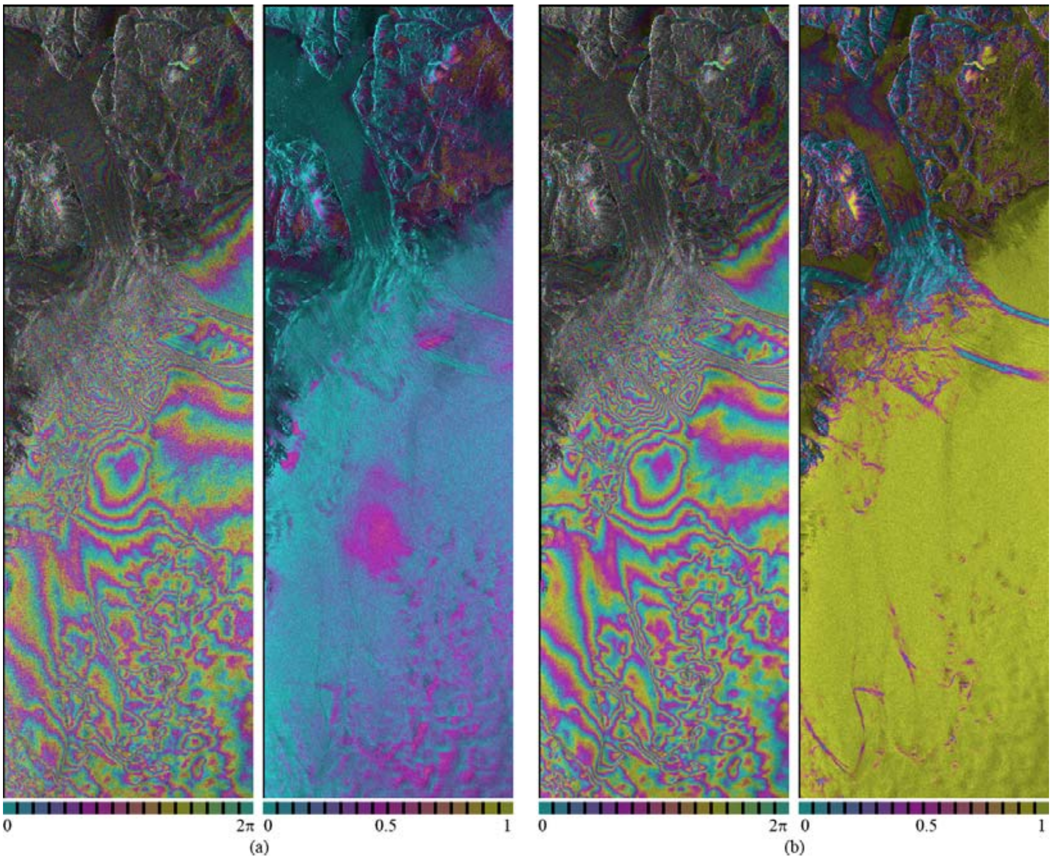

Figure 38. *Interferometric phase and coherence output by the IFF for T2 (a) without adaptive filtering (b) after "Goldstein" adaptive filtering.*

Since T2 exhibited a low coherence, processing was repeated using the so-called "Goldstein" adaptive filtering technique [3], which was very effective in reducing the phase noise. Results of both processing runs are shown in Figure 38.

For T1, interferometric phase is quite insensitive to topography, due to the small 4 m perpendicular baseline. Therefore phase variations in Figure 37 mostly correspond to displacement, although slow-varying trends apparent in the bedrock areas to the top-right of the image (Kronprins Christian Land), very likely due to orbit inaccuracies, and where steep topographic variations occur, as in the bedrock area in the left of the image (Lambert Land). Coherence for the T1 data set is exceptionally high on average, with expected low values at the shear margins and at the entrance of the fjord, where flow is turbulent and accompanied by topographic variations.

The T2 interferometric phase shows a much higher sensitivity to topography, due to the 105 m baseline, as can be noticed especially on bedrock. Coherence of the T2 data set, Figure 38, is not uniformly low, since some coherent patches are seen. This suggests the cause of decorrelation could be weathering (e.g. a snow-fall) between the two acquisitions, separated by 1 day.

Geophysical Inversion

The GIM was run to obtain height and slant-range displacement measurements from the T1 and T2 interferograms, and azimuth and slant-range displacement from the T1 offsets.

The external DEM from the reference height data set was used, and a set of 20 GCPs was extracted from the reference displacement data set, from areas at the sides of the main icestream. InSAR measurements were obtained with two techniques, namely DEM elimination, using either T1 or T2 and the external DEM, and Double Difference, using both the T1 and the T2 interferograms. Offset-tracking displacement measurements were derived from the results of intensity- and coherence-tracking. The results for each technique are described in the following subsections.

InSAR DEM Elimination

Within the GIM, a synthetic interferogram was generated from the reference DEM, and used to re-flatten the phase of the T1. Subsequently phase-unwrapping was carried out using the algorithm in [4]. A least-square fit to the expected phase from the GCPs was carried out, to calibrate out orbital and atmospheric effects. The resulting phase was converted to line-of-sight displacement, with a positive sign indicating motion towards the radar. Displacement measures were geocoded to a lat/lon grid (Equiangular projection), at a posting of 9 arcsec and 36 arcsec in latitude and longitude respectively, corresponding to roughly 250 m x 250 m on ground. The resulting geocoded line-of-sight velocity map is plotted next to the reference displacement map in Figure 39.

On the glacier tongue in Figure 39, no measurements were available, since unwrapping with the chosen algorithm failed across the low coherence area at the entrance of the fjord (See Figure 37). The velocity differences compared to the reference are plotted in Figure 40 (left). Some differences are very regular in shape, and are most likely due to the mosaicing process used to generate the reference velocities. These probably cause the distribution of the observed differences to deviate from the Gaussian one, Figure 40 (right). Elsewhere most of the differences lie within 4 m/y.

An independent error analysis was done computing the velocity statistics for bedrock areas in the top-left and top-right areas of Figure 39 (left), which are expected to be stationary. Mean biases of -1.39 m/y and -2.71 m/y and standard deviations of 0.28 m/y and 0.42 m/y were found respectively. The root-mean-square values of both comparisons could be explained by the following error budget:

- Decorrelation errors: 0.08 m/y (coherence=0.95) to 0.18 m/y (coherence=0.8), for 22 independent averaged phase samples.
- Atmospheric errors: 0.42 m/y (π/12 differential phase delay).
- Topographic compensation errors: 0.05 m/y (Bperp = 4 m, DEM accuracy = 13 m).
- Reference velocity errors: 3.0 m/y.

This would yield an expected displacement measurement error standard deviation in the order of 0.43 m/y.

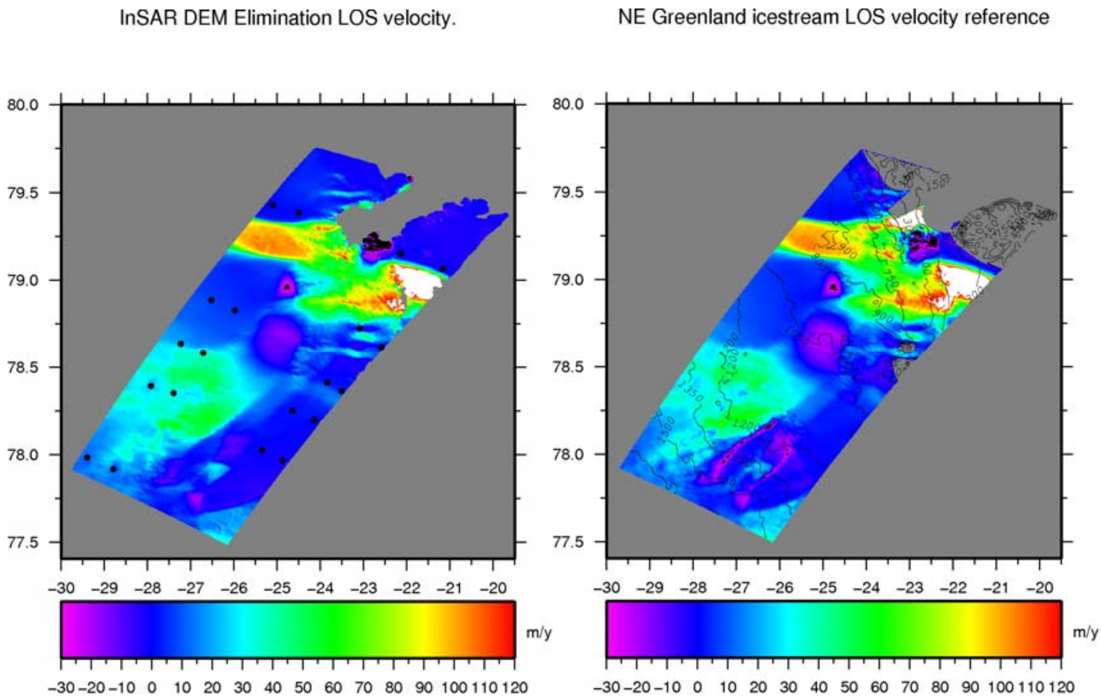

Figure 39. *Geocoded LOS velocity from GIM DEM elimination (left) and from the reference (right). Latitude and longitude degrees are reported on the y and x axis respectively.*

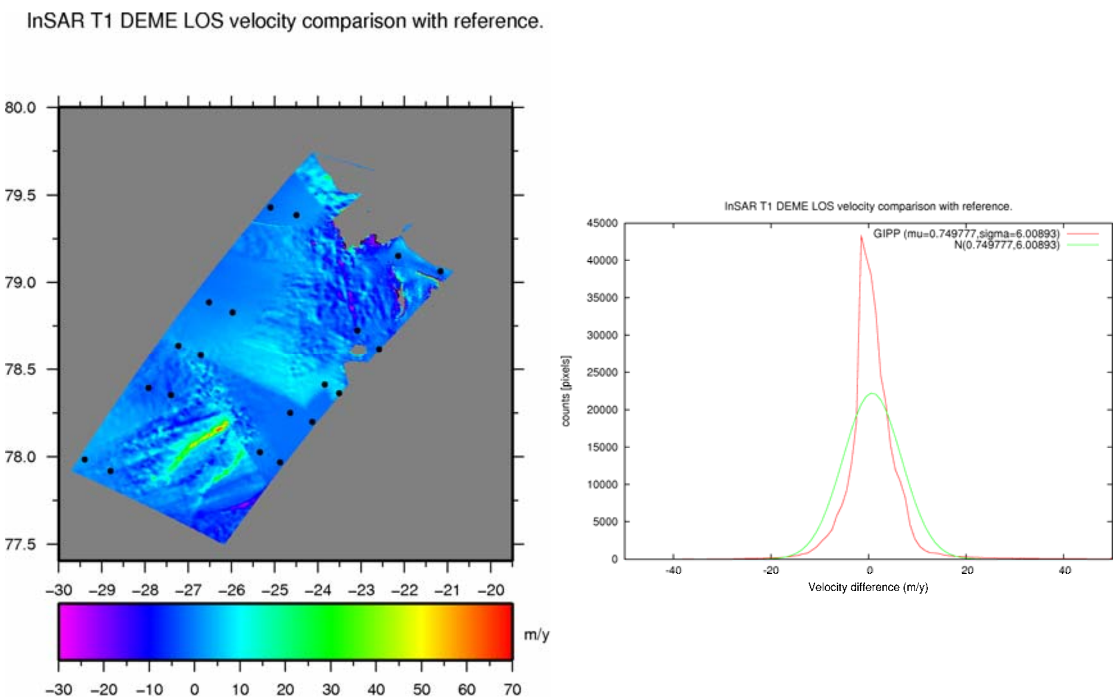

Figure 40. *Differential LOS velocity compared to the reference (left) and corresponding histogram (right). The red curve in the histogram refers to the actual difference measurements, whereas the superimposed green curve represents a Gaussian distribution with same mean and standard deviation.*

InSAR Double Difference

Interferograms T1 and T2 were processed with the GIM, using the Double Difference technique, obtaining geocode line-of-sight displacement and a height maps.

Processing differs from the DEM elimination method, in that topographic contribution from to the interferometric phase is estimated by differencing the two interferograms, assuming a common displacement rate. For this data-set topography is therefore estimated with a perpendicular baseline of about -4 m - 106 m = 110 m.

In principle no external DEM is required in the processing. However the external reference DEM was used to improve phase flattening, and thus aid phase unwrapping. The output height and displacement were geocoded to an equiangular projection, at a 250 m x 250 m posting, as for the DEM elimination results.

The measured LOS displacement, together with the measured height contours are shown in Figure 41 (left). The same plot for the reference data set is provided for comparison. The differences in height and displacement are shown in Figure 42. In Figure 41 and Figure 42 displacement is positive towards the radar, and elevation is referred to the WGS-84 ellipsoid.

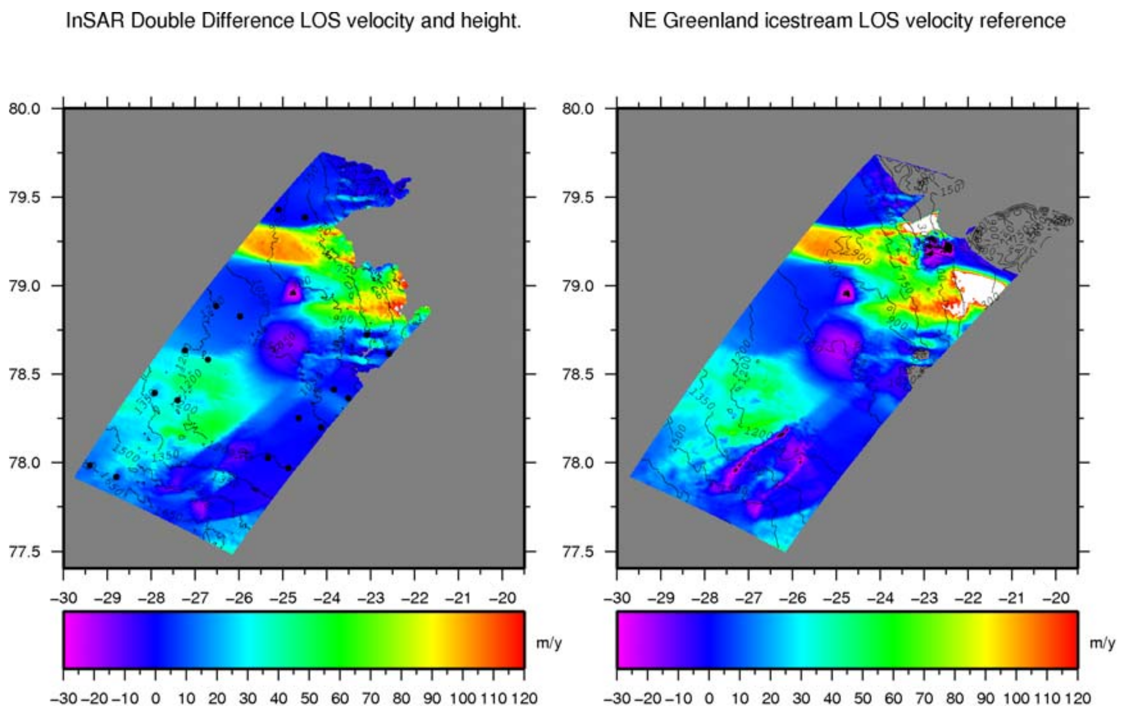

Figure 41. *DD results: LOS velocity from the GIM (left) and from the reference (right)*

The mean differences compared to the reference were 1.14 m/y and -5 m respectively, with standard deviations of 5.55 m/y and 39 m. In both cases the distributions were not Gaussian, as can be seen from the images of Figure 42. An error budget based on the sensitivity equations of the Double-Difference method yields an expected height standard deviation of 21 m, and an expected displacement error of 0.58 m/y. These figures, together with the accuracy of the reference data, were considered sufficient to explain the observed differences.

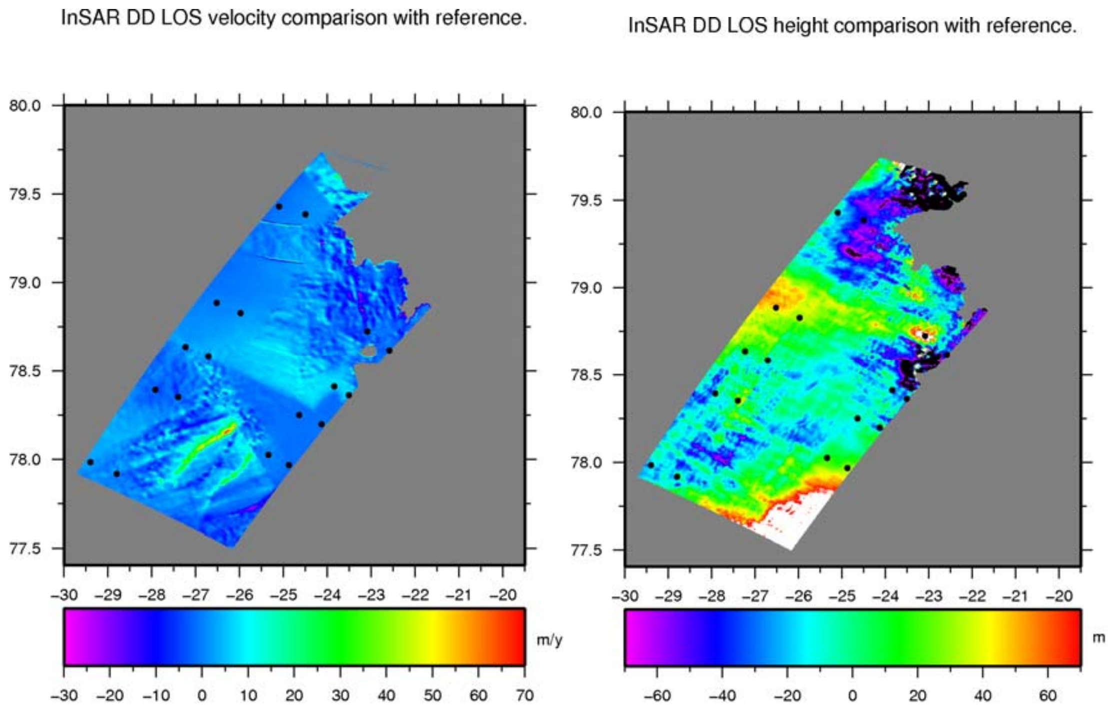

Figure 42. *DD results: Differential LOS velocity (left) and height (right) with respect to the reference.*

Coherence-Tracking Velocities

The GIM was used on the output of the T1 OTR coherence-tracking run, described in a previous section. Geocoded line-of-sight and azimuth displacement maps were generated.

Within the GIM, the slant range and azimuth offsets output by the OTR were calibrated, using ground control points, before being converted to displacement. The azimuth and range offset error throughout the image was modelled as a plane (3 parameters), and the model parameters were estimated in a least-square sense based on the observed and the expected offsets at the control points. An iterative procedure was use to discard points which differed from the median by more than 3.5 times the inter-quartile range. The estimated polynomial corrections were subtracted from the offset measurements. This calibration procedure was not part of the GAMMA software package, and was implemented as an auxiliary C program.

Subsequently the offsets were converted to displacements in the line-of-sight and in azimuth by applying the appropriate scaling factors, depending on pixel size (4 m x 8 m respectively for ERS), grid dimensions (10 x 50) and temporal baseline (1 day for Tandem data).

Finally measurements were geocoded on a 9 x 36 arcsec posting in latitude and longitude respectively. The results are shown in Figure 43, whereas a comparison with the reference displacement measures is provided in Figure 44 and Figure 45.

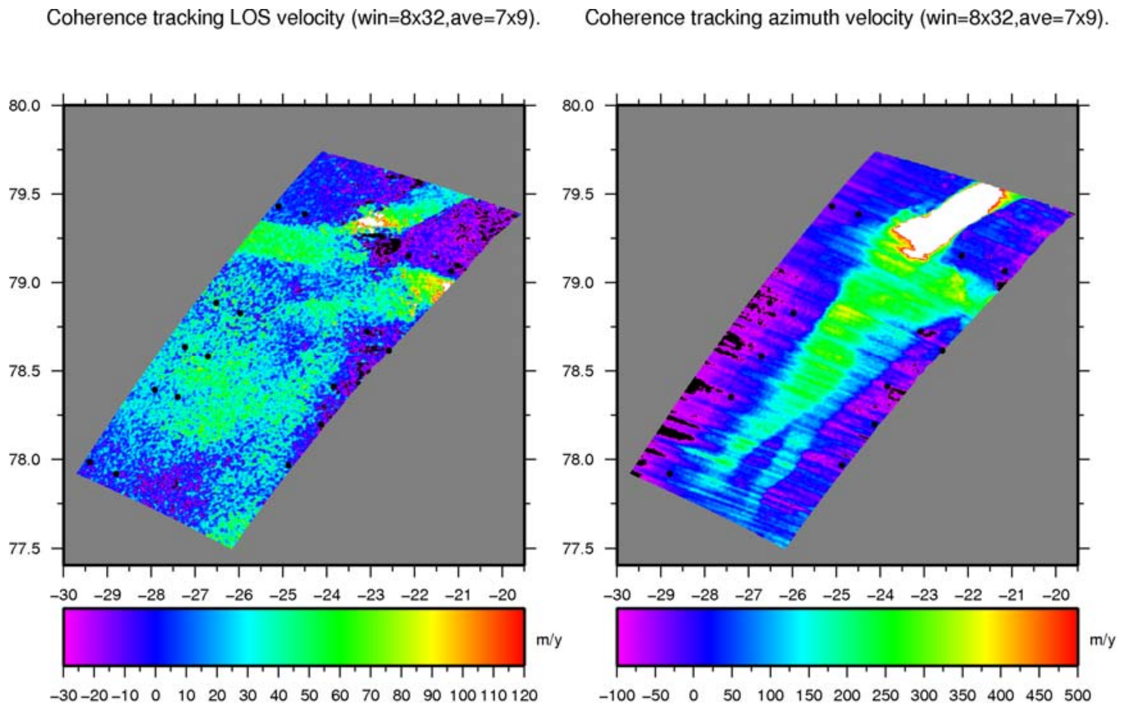

Figure 43. *Coherence tracking: geocoded LOS velocity (left) and azimuth velocity (right).*

The line-of-sight velocity map appears noisy compared to the corresponding ones, derived with InSAR techniques (See Figure 39 and Figure 41). A bias is also apparent in the high-velocity areas in the upper part of the image. This is very likely due to an improper offset-calibration. In fact 3 control points were discarded in the calibration procedure, resulting in a weak conditioning of the right portion of the velocity map. The calibration procedure is not robust in the face of noise, since it does not take error standard deviations or correlations into account. This issue will be addressed in WP-3.

The RMS error in the line-of-sight is in the order of 30 m/y compared to the reference, as seen from Figure 45. This value however is somewhat misleading, as the histogram of the differences seems to contain two overlapping Gaussian bells, centred on different mean values. These are likely to correspond to the upper and lower part of the image respectively. On two bedrock areas in the top-left and top-right of Figure 43, RMS deviations of 8 m/y were found.

The error budget expected from theory in areas of high coherence ranges between 6.5 m/y and 11.4 m/y for coherences in the range of 0.9 to 0.75 respectively. These values are based on the curves reported in Fig. 1 in [5], and on the correlation windows and averaging factors used in the OTR processing. These expectations are considered in sufficiently good agreement with the bedrock observations.

The azimuth displacement map, Figure 43 (right), is dominated by the ionospheric effects already noted in a previous section. In this case the latter indirectly cause a large additional bias, by inducing an error in offset calibration. RMS azimuth velocities on bedrock were found to be about 16 m/y. Azimuth displacement accuracy expected theoretically is in the order of 3 to 6 m/y, since the azimuth pixel-spacing is smaller than the slant-range one by a factor 2. It is therefore likely that ionospheric effects contribute the additional unexplained variance of about 10 to 13 m/y, corresponding roughly to 0.01 azimuth pixels. This error figure agrees with other observations [6].

Methods have been proposed to remove ionospheric effects [7], [8], but the procedure requires care, especially when the scene presents a high motion component in the azimuth direction, as is the case at hand. Therefore it was considered out of the scope of this work.

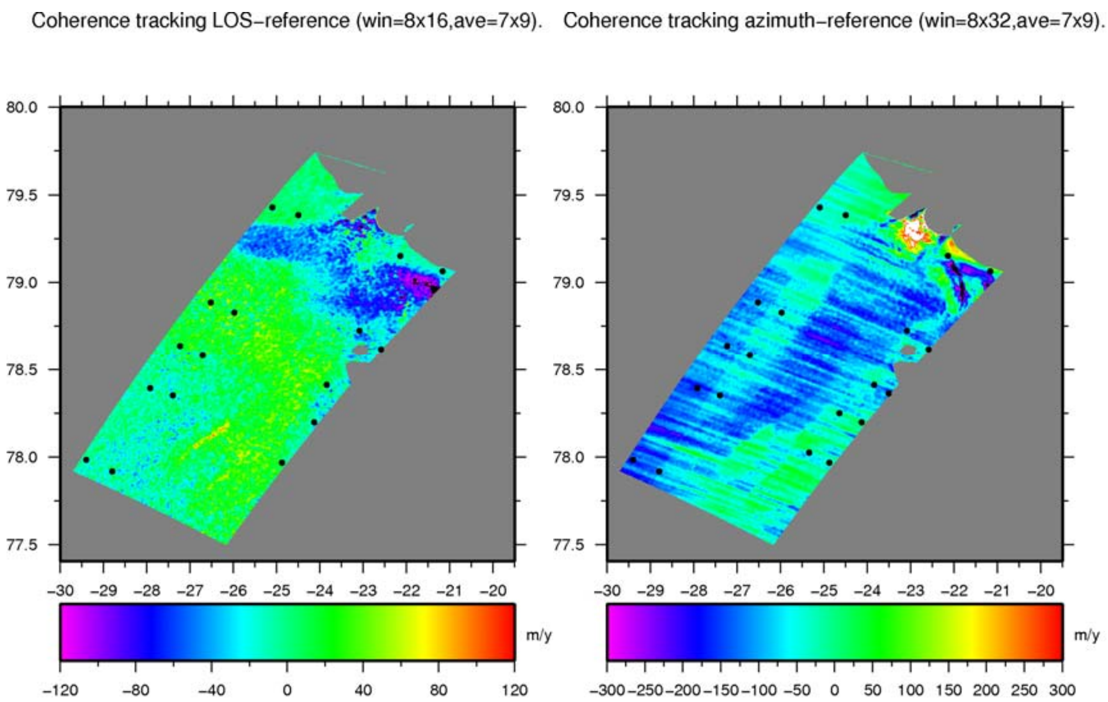

Figure 44. *Coherence tracking: Differential LOS velocity (left) and azimuth velocity (right) with respect to the reference. Areas in black and white exceed respectively the lower and upper boundary of the colour scale.*

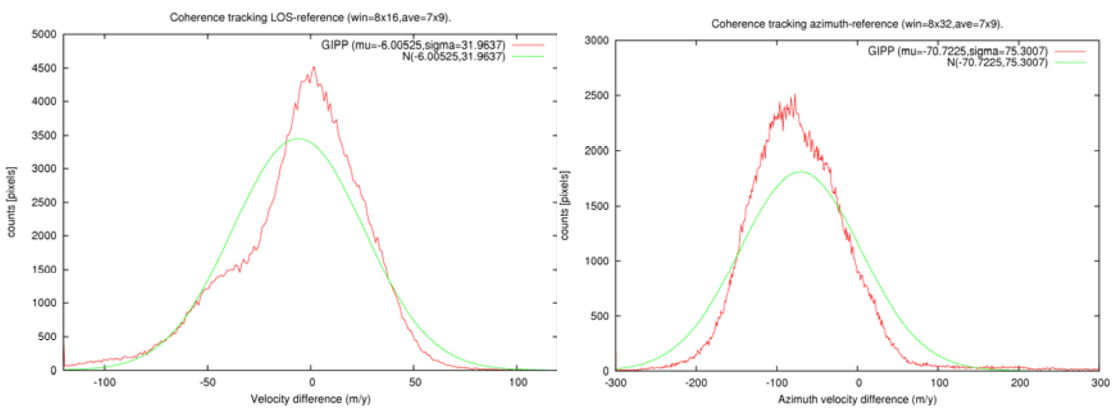

Figure 45. *Coherence tracking comparison: LOS velocity (left) and azimuth velocity (right) differences compared to the reference data set. The red curve corresponds to the actual differences, whereas the superposed green curve represent a Gaussian distribution with same mean and standard deviation.*

Intensity-Tracking Velocities

The GIM was used on the output of the OTR intensity-tracking run on the T1 SLC-pair, described in a previous section. The same offset calibration procedure described in the previous section was applied. Finally measurements were geocoded on a 9 x 36 arcsec posting in latitude and longitude respectively. The results are shown in Figure 46, whereas a comparison with the reference displacement measures is provided in Figure 47 and Figure 48.

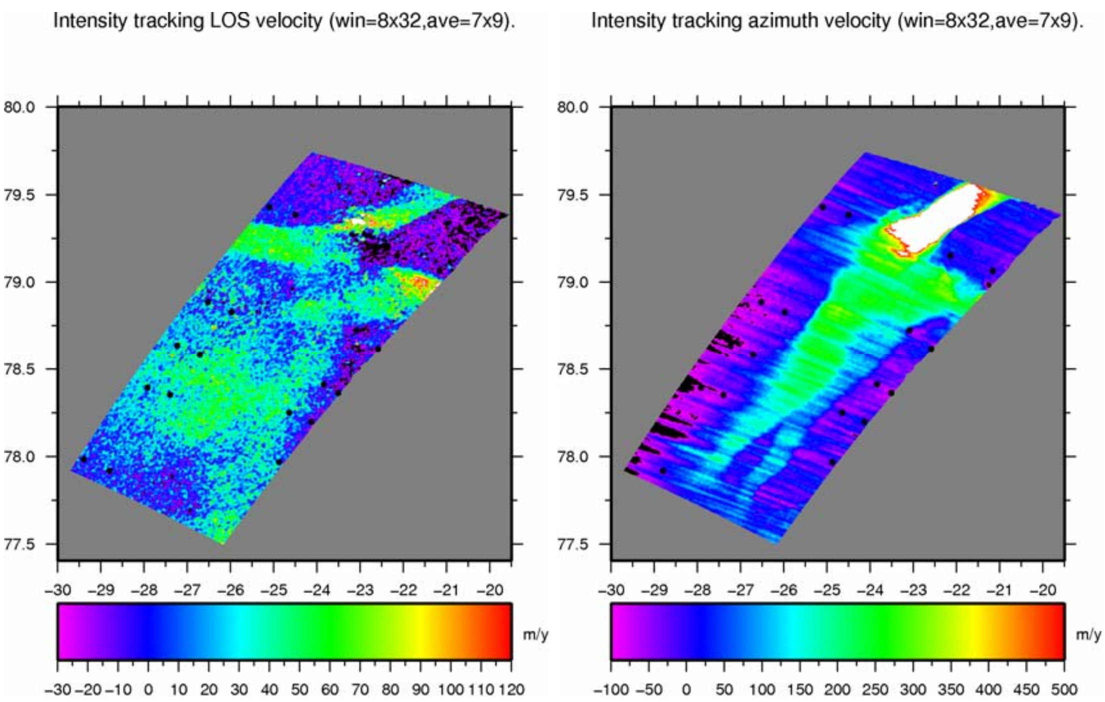

Figure 46. *Intensity tracking: LOS velocity (left) and azimuth velocity (right).*

Similar results compared to coherence-tacking were obtained. RMS velocities on bedrock were found to be around 11 m/y in slant-range and about 20 m/y in azimuth. The expected errors are within 6.5 and 11.3 m/y in slant-range and half of these values in azimuth. The observations on bedrock are explained, assuming ionospheric effects to contribute an additional variance of about 10 to 13 m/y, as for the coherence-tracking results.

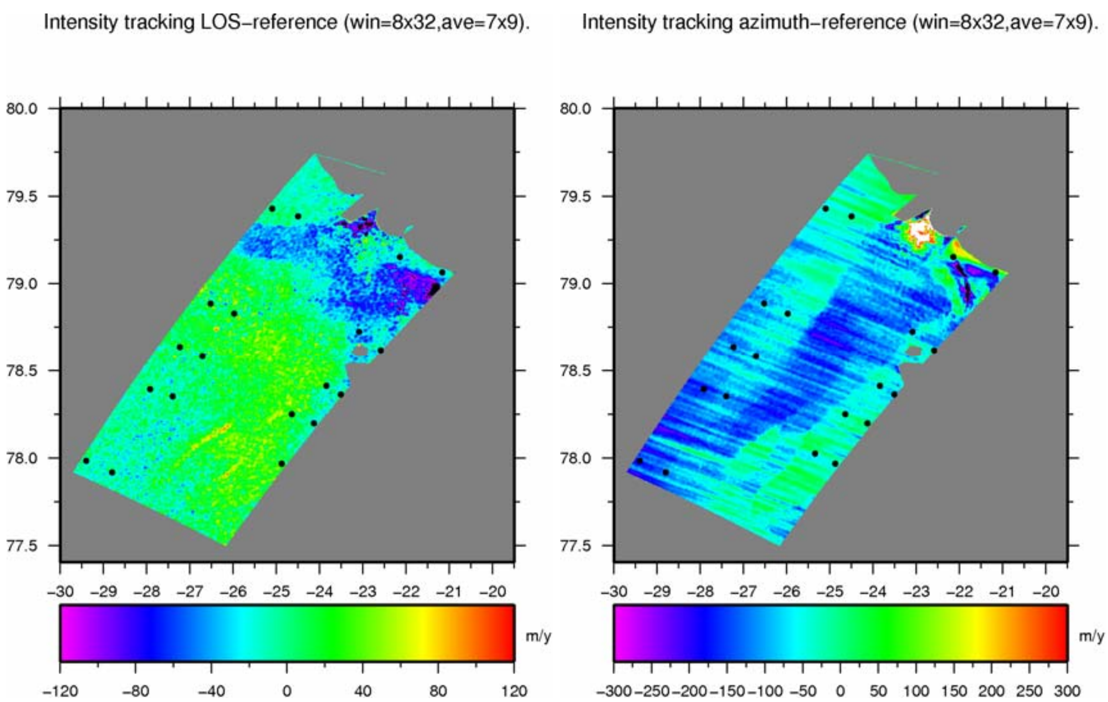

Figure 47. *Intensity tracking: LOS velocity (left) and azimuth (right) velocity differences with respect to the reference.*

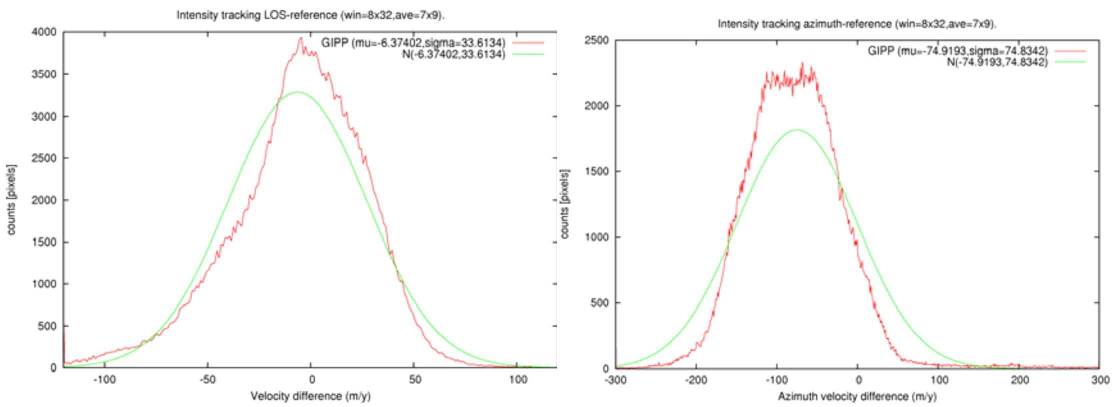

Figure 48. *Intensity tracking comparison: LOS velocity (left) and azimuth velocity (right) differences compared to the reference data set. The red curve corresponds to the actual differences, whereas the superposed green curve represent a Gaussian distribution with same mean and standard deviation.*

References

[1] I.R. Joughin, M.A. Fahnestock, J.L. Bamber, “Ice flow in the northeast Greenland ice stream”. *Ann. Glaciol.*, 31, pp. 141-146, 2000.

[2] A.L. Gray, K.E. Mattar, G. Sofko, “Influence of ionospheric electron flux on satellite radar interferometry”, *Geophys. Res. Lett.*, Vol. 27, No. 10, pp. 1451-1454, 2000.

[3] R.M. Goldstein, C.L. Werner, “Radar interferogram filtering for geophysical applications”, *Geophys. Res. Lett.*, Vol. 25, No. 21, pp. 4035-4038, 1998.

[4] R.M. Goldstein, H.A. Zebker, C.L. Werner,”Satellite radar interferometry two-dimensional phase unwrapping”, *Radio Sci.*, Vol. 23, No. 4, pp. 713-720, Jul./Aug. 1988.

[5] R. Bamler, M. Eineder, “Accuracy of differential shift estimation by correlation and split-bandwidth interferometry for wideband and Delta-k SAR systems”, *IEEE Geosc. Rem. Sens. Lett.*, Vol. 2, No. 2, Apr. 2005.

[6] I. Joughin, “Ice-sheet velocity mapping: a combined interferometric and speckle-tracking approach”, *Ann. Glaciol.*, 34, pp. 195-201, 2002.

[7] K.E. Mattar, A.L. Gray, “Reducing ionospheric electron density errors in satellite radar interferometry applications”, *Can J. Rem. Sens*, Vol. 28, No. 4, pp. 593-600, 2002.

[8] U. Wegmuller, C.L. Wrner, T. Strozzi, A. Wiesmann, “Ionospheric electron concerntration effects on SAR and InSAR”, *In Proc. IGARSS’06*, 2006.

zs